

MICROCOPY RESOLUTION TEST CHART  
NATIONAL BUREAU OF STANDARDS-1963-A



TR-85-069

AD: /

Final Report  
for the period  
November 1983 to  
April 1985

# Multi-Stage Plasma Thruster

June 1987

Author:  
P. Turchi

R & D Associates  
Washington Research Laboratory  
301A S. West St.  
Alexandria, VA 22314

RDA-TR-127600-001  
F04611-83-C-0033

AD-A183 635

Approved for Public Release

Distribution is unlimited. The AFRPL Technical Services Office has reviewed this report, and it is releasable to the National Technical Information Service, where it will be available to the general public, including foreign nationals.

DTIC  
ELECTE  
AUG 17 1987  
S D E

prepared for the: **Air Force  
Astronautics  
Laboratory**

Air Force Space Technology Center  
Space Division, Air Force Systems Command  
Edwards Air Force Base,  
California 93523-5000

87 8 13 10 4

A183635

REPORT DOCUMENTATION PAGE

1a. REPORT SECURITY CLASSIFICATION UNCLASSIFIED		1d. RESTRICTIVE MARKINGS	
2a. SECURITY CLASSIFICATION AUTHORITY		3. DISTRIBUTION/AVAILABILITY OF REPORT Approved for Public Release. Distribution is Unlimited.	
2b. DECLASSIFICATION/DOWNGRADING SCHEDULE		5. MONITORING ORGANIZATION REPORT NUMBER(S) AFRPL-TR-85-069	
4. PERFORMING ORGANIZATION REPORT NUMBER(S) RDA-TR-127600-001		7a. NAME OF MONITORING ORGANIZATION Air Force Astronautics Laboratory	
6a. NAME OF PERFORMING ORGANIZATION R & D Associates	6b. OFFICE SYMBOL (If applicable)	7b. ADDRESS (City, State and ZIP Code) AFAL/LKCJ Edwards AFB 93523-5000	
6c. ADDRESS (City, State and ZIP Code) Washington Research Laboratory 301A S. West Street Alexandria, VA 22314		9. PROCUREMENT INSTRUMENT IDENTIFICATION NUMBER F04611-83-C-0033	
8a. NAME OF FUNDING/SPONSORING ORGANIZATION	8b. OFFICE SYMBOL (If applicable)	10. SOURCE OF FUNDING NOS.	
8c. ADDRESS (City, State and ZIP Code)		PROGRAM ELEMENT NO. 62302F	TASK NO. 00
11. TITLE (Include Security Classification) MULTI-STAGE PLASMA THRUSTER (U)		PROJECT NO. 5730	WORK UNIT NO. IQ
12. PERSONAL AUTHOR(S) Turchi, Peter			
13a. TYPE OF REPORT Final	13b. TIME COVERED FROM 83/11 TO 85/4	14. DATE OF REPORT (Yr., Mo., Day) 87/6	15. PAGE COUNT 66
16. SUPPLEMENTARY NOTATION			
17. COSATI CODES		18. SUBJECT TERMS (Continue on reverse if necessary and identify by block number)	
FIELD 21	GROUP 03	Electric Propulsion, Plasma Systems, Electrical Engines.	
19. ABSTRACT (Continue on reverse if necessary and identify by block number) Multi-stage plasma propulsion offers the opportunity to extend electric propulsion capabilities as space power levels develop. In this effort, the contractor considered an electric propulsion development strategy in which a family of thrusters was based on multiple stages of electromagnetic acceleration using the Teflon pulsed plasma thruster as the initial stage. Experimental tests explored three multi-stage thruster configurations. The contractor concluded that multi-stage can match mission power levels and transfer times.			
20. DISTRIBUTION/AVAILABILITY OF ABSTRACT UNCLASSIFIED/UNLIMITED <input checked="" type="checkbox"/> SAME AS RPT <input type="checkbox"/> DTIC USERS <input type="checkbox"/>		21. ABSTRACT SECURITY CLASSIFICATION UNCLASSIFIED	
22a. NAME OF RESPONSIBLE INDIVIDUAL Robert D. Meya, 1Lt, USAF		22b. TELEPHONE NUMBER (Include Area Code) (805) 275-5473	22c. OFFICE SYMBOL AFAL/LKCJ

DRAFT FINAL REPORT TO AFRPL

MULTI-STAGE PLASMA THRUSTER

	PAGE
I. SUMMARY	1
II. INTRODUCTION	3
III. APPROACH	8
IV. THEORETICAL STUDIES	14
V. EXPERIMENTAL TESTS	24
VI. CONCLUSIONS	38
VII. REFERENCES	40
VIII. APPENDICES	
A. PULSED PLASMA THRUSTERS FOR ORBIT TRANSFER	41
B. SAMPLE DESIGN OF A TWO-STAGE THRUSTER	49
C. CRITICAL SPEED FOR SELF-FIELD PLASMA THRUSTERS	55

Accession For	
NTIS GRA&I	<input checked="" type="checkbox"/>
DTIC TAB	<input type="checkbox"/>
Unannounced	<input type="checkbox"/>
Justification	
By _____	
Distribution/	
Availability Codes	
Dist	Avail and/or Special
A-1	



## LIST OF FIGURES

<u>FIGURE</u>	<u>CAPTION</u>	<u>PAGE</u>
1	Schematic of Pulsed Plasma Thruster	9
2	Conceptual Designs for Second-Stage Acceleration	9
3	RDA Advanced Thruster Research Family of Thrusters from PPT	11
4	Conceptual diagrams of plasma injection from PPT into second-stage thruster	15
5	Results from normalized lumped-circuit calculations	17
6	Expansion of a semi-infinite magnetized plasma into a field-free vacuum	19
7	Expansion and recollection of a plasma slab driven by a constant magnetic field	21
8	Sectional view of Experimental Thruster Facility at the RDA Washington Research Laboratory	25
9	Schematic diagram of long-rail experimental set-up	26
10	Sectional view of second-stage in Short Rail Experiments	26
11	Current vs time for the Short Rail Experiments with 5kV on Pulse Forming Network	30
12	Voltage vs Time for the Short Rail Experiments with $V_0 = 5$ kV initial voltage on PFN	30
13	Langmuir Probe Ion Saturation Current vs Time for the Short Rail Experiments $V_0 = 5$ kV	32
14a	Current vs Time for the Inlet-Rail Experiments with $V_0 = 15$ kV	35
14b	Voltage vs Time for the Inlet-Rail Experiments with $V_0 = 15$ kV.	
15	Langmuir Probe Ion Saturation Current vs Time 40 cm from Exit with $V_0 = 15$ kV	36

## I. SUMMARY

Although electric propulsion has been recognized for several decades as the appropriate technique for achieving orbital transfers with minimum fuel expenditures, it has not had significant use in actual space missions. A primary factor in the selection of propulsion systems is flight experience. Such experience, however, cannot be accumulated unless initial use is made of a system in space, which requires either an overwhelming need for new technology or a limited need in a relatively low risk mission. The former requirement usually cannot occur without imperiling the proposed mission; the latter need existed in selection of the pulsed plasma micro-thruster (PPT) for satellite station-keeping. An electric propulsion development strategy is considered in which a family of thrusters is based on multiple stages of electromagnetic acceleration utilizing the PPT as the initial stage.

Theoretical studies indicate the ability of second-stage acceleration to provide higher specific impulse and thrust efficiency using the PPT exhaust as a source of plasma mass. Doubling of the plasma speed, with thrust efficiencies in excess of 50 percent appear possible. Studies also consider the use of the PPT exhaust to initiate an ablation arc in the second-stage thruster, thereby providing higher total thrust at useful specific impulse levels (1000-1500 sec). A sample design is presented (Appendix B) in which a pulse forming network (PFN) is matched to a second-stage quasi-steady ablationfed thruster at 1500 sec and 10 mlb average thrust level. Elementary system calculations (Appendix A) indicate that such a design configuration could deliver up to 60 percent of the initial spacecraft mass from LEO-to-GEO (assuming 80 percent of the power system is part of the mission payload).

Experimental tests explored three multi-stage thruster configurations, comprising pulsed acceleration of PPT plasma to  $4 \times 10^4$  m/s by a long second-stage, and quasi-steady ablation of additional Teflon plasma in second-stages with short

electrodes. The latter thrusters provide plasma speeds of  $1.7-2.5 \times 10^4$  m/s with nearly constant average particle fluxes for the duration of the PFN current pulse (150  $\mu$ sec after the PPT transient). It appears that variation of total impulse by changing the current pulsetime can permit multi-stage thrusters to match available mission power levels and transfer times.

The notion of a critical limiting exhaust speed for self-field electromagnetic thrusters is examined (Appendix C) using a model in which convective cooling by propellant flow and ablation balances resistive heating. At a speed that can be close to Alfvén critical speed, ablation is necessary to cool the thruster and may result in a velocity "plateau". Voltage oscillations associated with flow speed fluctuations can occur if the efficiency of heat transfer from the plasma to ablation involves a scale size comparable to that for current density variation. The use of exothermic vs endothermic propellant slabs is also considered, with the principal difficulty resulting from loss of electrical conductivity at high chamber pressure.

Multi-stage plasma propulsion offers the opportunity to extend electric propulsion capabilities as space-power levels develop, building on a common base of operational experience and thruster physics.

## II. INTRODUCTION

"Electric propulsion systems have found growing attention during recent years"

E. Stuhlinger, 1964 (Ref. 1)

At the time of Dr. Stuhlinger's remarks, numerous techniques<sup>2</sup> had been proposed by which spacecraft could be propelled electrically. During the subsequent three decades, significant advances have been made in the laboratory to broaden the range of applicability of electrostatic engines to lower specific impulse values (perhaps as low as 2000 sec<sup>3</sup>), and to extend arcjet performance from the early arc-heater regime of 800-1000 sec up to 1500-2000 sec at low density and high power<sup>4</sup>. In all this time, however, the only electric thruster applied in a US mission has been the pulsed plasma microthruster or PPT<sup>5</sup>, a device of rather modest performance and sophistication compared to ion engines and MPD accelerators. In view of the "growing attention" possibly recurring in electric propulsion, it is useful to consider features of the PPT that have enabled it to enter the inventory of operational spacecraft propulsion systems, while other devices have remained in the laboratory. Such consideration indicates important physical and programmatic elements that should be retained in attempting to introduce higher performance techniques into the operational inventory, and thereby suggests a strategy for electric propulsion development.

### II.1. FACTORS IN ELECTRIC PROPULSION USE

It is well known that electric propulsion techniques offer high specific impulse and thereby can achieve trajectory changes with significantly higher payload mass fractions than chemical propulsion systems, if long duration, low thrust levels are allowed by mission constraints. A simple expression that summarizes most of the basic concerns associated with electric propulsion mission analysis is the formula for optimum exhaust speed<sup>6</sup>:

$$u_0 = \sqrt{K \frac{P}{m}}$$

where  $k$  is a number between one and two, depending on the ratio of  $u_0$  to the desired payload velocity change  $\Delta v$ ,  $\alpha$  is the ratio of input power to power supply and engine mass,  $\eta$  is the efficiency of conversion of input power to thrust power, and  $\tau$  is the thrust duration. The factor  $\alpha$  is a slight generalization of the usual specific power (reflecting an expectation that thruster mass will be proportional to power to the same extent that power supply mass scales with power). The so-called power supply penalty for electric propulsion is readily apparent when values of  $u_0$  are calculated (Table I) for an optimistic choice of specific power ( $\alpha = 200$  w/kg), a thrust efficiency  $\eta = 50\%$ , and a mission constant  $k = 1.5$ .

Table I

Optimum Exhaust Speeds

( $\alpha = 200$  w/kg,  $\eta = 0.5$ ,  $k = 1.5$ )

<u><math>\tau</math></u>	<u><math>u_0</math> m/sec</u>	
1 hour	735	Chemical Thrusters
1 day	3,600	
10 days	20,000	Electromagnetic Thrusters

For short duration missions, which may be interesting for defensive maneuvering, the optimum exhaust speed for an electric thruster can be readily achieved by conventional techniques (chemical combustion, or even nitrogen jets for very quick changes). If a month is available for the trajectory change, however, then the optimum exhaust speed is beyond the capability of chemical systems, so electric propulsion would be justified (within assumed parameters that include a desired  $\Delta v$  comparable to the exhaust speed). For longer mission times, associated with LEO-to-GEO or LEO-to-lunar transport of supplies and equipment, it is easier to justify electric propulsion. Such longer times, however, require reliable operation of all thruster and power supply components, since backup supply or retrieval could be very difficult. (Recovering an errant EP-driven space tug could be an interesting, albeit embarrassing, electric propulsion mission).

Shorter duration missions may also be appropriate for electric propulsion if a substantial portion of the power supply is needed by the mission payload. Delivery of power supplies to synchronous space stations or lunar bases might be needed, for example. If a fraction  $f$  of the power supply and thruster mass is associated only with propulsion, then the optimum exhaust speed is:

$$u_0 = \sqrt{k\alpha n \tau / f}$$

Table II provides sample values for  $f = 0.1$  to indicate the effect of power-intensive payloads on various missions. Note that mission times of less than one day may be appropriate for electric propulsion. Substantial changes in satellite orbits could, therefore, be achieved efficiently in several orbits. Earth-local maneuvering missions (vs deep-space probes) may provide relatively near-term requirements for electric propulsion in the specific impulse range of 1000-1500 sec.

Table II

Optimum Exhaust Speeds for Power-Intensive Missions

( $\alpha = 200$  w/kg,  $\eta = 0.5$ ,  $k = 1.5$ , and  $f = 0.1$ )

<u><math>\tau</math></u>	<u><math>u_0</math> (m/sec)</u>	
1 hour	2,300	Still Chemical
1 day	11,000	Electro Thermal/Magnetic
30 days	63,300	Electromagnetic Electrostatic

II.2. ELECTRIC PROPULSION DEVELOPMENT

There have been three basic reasons for the limited use of electric propulsion. The techniques developed to apply electrical energy often have had quite low thrust density and supportance, so the acceleration profile did not satisfy mission constraints; the mass of electrical power supply becomes too large a fraction of the total payload; and last, but not least, it is difficult to displace an established technology even if considerable intrinsic advantage can be claimed for the new technology. The first two reasons are closely related and depend on the progress of technology and mission requirements.

The last reason tends to be independent of technology and requires consideration of strategy. (As previously noted, there are dozens of electric thruster schemes that have not flown, regardless of their specific impulse advantage over cold nitrogen or hydrazine).

If the development of space technology two decades ago had required large electrical power supplies for missions such as communications, surveillance, weaponry, etc., then electric thrusters might have flown early enough in the program to accumulate flight time comparable to chemical systems. Developments in electronics and data-processing, however, removed much of the need for substantial electrical power even for the deep-space missions (previously cherished by electric propulsion enthusiasts). With the considerable cost of launching systems into space, the emphasis was on small, extremely reliable devices. Little room was available for electric propulsion tests and evaluation. The advent of the Space Transportation System, however, may have changed the outlook for launching systems that are large (and include substantial power supplies) and that may require maintenance after long periods of operation in space. The opportunity may now exist for a fresh start on electric propulsion for spacecraft. It must be recognized in attempting such a start that standards of reliability will still be imposed that, at least for the first electric thrusters, will preclude many schemes that are conceptually satisfactory, even laboratory-tested, but are not flight-qualified. The historical pitfall of devoting effort and resources to a thruster scheme that is developed in the laboratory, only to remain there, should be avoided.

### II.3. THE PULSED PLASMA THRUSTER

Pulsed plasma thrusters have been proposed in various forms including "button guns", coaxial shock tubes, plasma rail guns, conical theta pinches, etc. Some use ablation of films or surfaces, others involve breakdown of gaseous propellants. The timescales of operation range from submicro-

second to many milliseconds (quasi-steady). Of all the variants, the one that flew was based on a triggered spark discharge across a Teflon block. The characteristics of this thruster, including analyses of the exhaust products, speeds, impulse bits, scaling laws, and flight use, are documented in References 5, 7-10. Briefly, discharge of a capacitor provides 1-2 J in the vicinity of the surface of a Teflon block that is fed between two electrodes by spring force. A portion of the surface ablates with the earliest material receiving most of the electrical energy, achieving multiple ionization states and speeds of a few  $\times 10^4$  m/sec. Even after the capacitor has discharged, sufficient hot plasma exists to continue ablation of the surface, resulting in a largely neutral, relative slow gas expansion ( $\sim 3$  km/sec). During the first few  $\mu$ sec, plasma densities are  $10^{15}$ - $10^{17}$   $\text{cm}^{-3}$  and ion temperatures may be several volts. The total mass ablated per shot is about  $10^{-8}$  kg, providing an impulse bit of about 30  $\mu\text{N}\cdot\text{sec}$ . The thrust efficiency is only a few percent, with about 30% of the energy lost in the capacitor itself. While there is certainly room for improvement in terms of the intrinsic behavior of the plasma acceleration event, the attention to system characteristics such as power supply and conditioning, packaging, and fuel handling proved sufficient to allow flight-qualification.

One reason for the successful introduction of the PPT into operational use is that its specific impulse is in approximately the proper regime to avoid significant power supply penalty for long duration missions (with less optimistic values of  $\eta$  and  $\bar{m}$  than used in Table I). Specific impulse advantage alone, however, is insufficient to displace existing technology (e.g., nitrogen or hydrazine). Two factors are probably most critical: simplicity and operational experience. The PPT includes the first factor in the use of solid propellant fed by a simple spring (see Fig. 1), instead of gas-valving (and associated tankage). High voltage switching is handled with a small trigger electrode to initiate the discharge across the face of the propellant slab, and the main power input is merely

a capacitor ring-down. The price of simplicity in the PPT is a nonconstant, nonuniform delivery of energy and momentum to the discharge plasma, (which results in the relatively low efficiency and broad distribution of exit plasma speeds. In the programmatic decision process, however, simplicity of operation is more important than intrinsic efficiency. This decision process thus allows a device of modest performance to obtain the operational experience that is crucial to further use. Such use then permits the development of improved models that can draw upon the operational accomplishment of their predecessors for support during research phases and for acceptance into the operational inventory.

### III. APPROACH

While it is possible to design and develop a plasma thruster capable of achieving  $I_{sp}$  values in the range of 1500 sec, with higher efficiencies than the PPT and perhaps even including some features of PPT design philosophy, it is probably necessary to preserve the line of operational experience by evolving a design from the PPT itself, rather than starting from basic principles. Such evolution may appear to be quite pedestrian. For example, the power circuitry can be improved by inclusion of passive network elements to match the time-varying discharge impedance. Development of larger-size versions of the pulsed plasma microthruster is also possible (and has been accomplished<sup>11</sup>). Such development, however, could break the connection with the operational experience of system components, if active portions of the power supply and thruster are modified for higher current, energy, and mass flow.

A different approach to the development of the PPT could allow the line of experience to be preserved by restricting the complicated portions of the thruster system to the existing PPT and extending performance by secondary stages of mass addition and plasma acceleration, designed with passive elements for simplicity of operation. Schematic representatives of such secondary stages are shown in Fig. 2 with a PPT providing

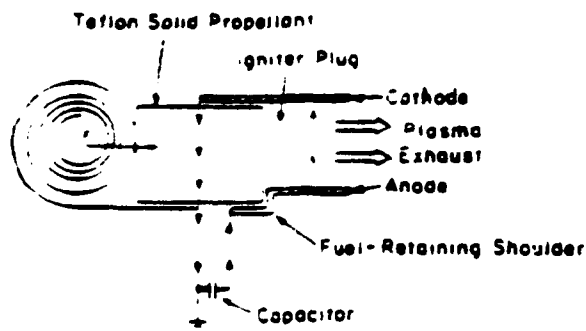


Fig. 1 Schematic of Pulsed Plasma Thruster (from Ref. 5)

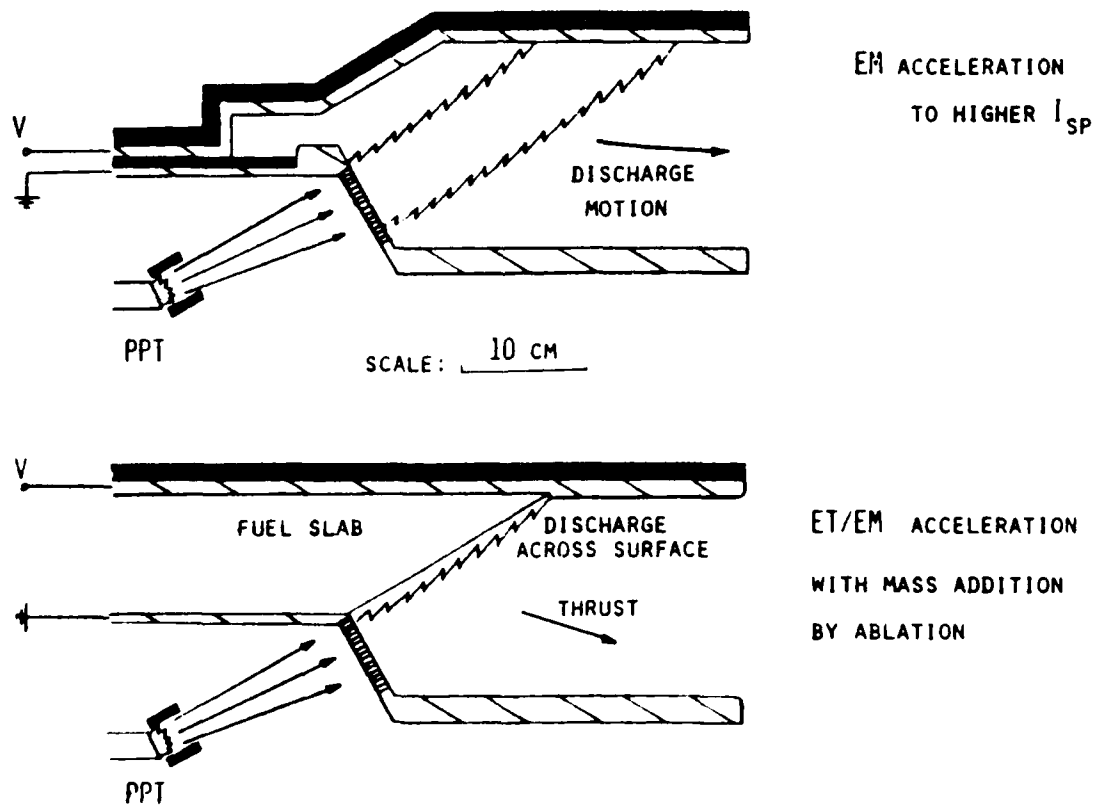


Fig. 2 Conceptual Designs for Second-Stage Acceleration.

plasma between two charged electrodes, in one case for further electromagnetic acceleration and in the other for mass addition by initiating discharge ablation in the second stage.

The factors for electric propulsion use that appear critical are concentration on more modest  $I_{sp}$  values consistent with near-term missions, and simplicity of thruster system design (e.g., fuel handling, power processing), even at the expense of significant intrinsic performance loss in order to maintain a record of operational accomplishment. The approach proposed consists of starting with the pulsed plasma microthruster and developing a family of electric thrusters that would eventually even include steady MPD arcjets and electric/chemical hybrid thrusters.

### III.1. A FAMILY OF ELECTRIC THRUSTERS

The possibility of a family of electric thrusters based on the pulsed plasma microthruster derives from the rather continuous mix of electrothermal and electromagnetic components of thrust in the 1000-2000 sec specific impulse regime, and recognition that much of the intrinsic physics of plasma acceleration is independent of the operating pulsetime. (Such similarity in physics allowed pulsed plasma thruster research based on 5  $\mu$ sec plasma implosions to convert rapidly to quasi-steady MPD arcjet studies with successively longer current pulses of 0.1 to 1 msec). Figure 3 shows the proposed connections between various family members grouped in terms of the stage of operation and the desire for greater exhaust or thrust. The first stage is the PPT, which contains the more complicated portions of the system (triggers, actively-pulsed circuits, etc.) and provides the initial plasma flow. This plasma flow has two distinct characteristics: mass and electrical conductivity. The PPT provides a pulse of mass, with a nonuniform velocity distribution, that can be injected into a second-stage for further acceleration. Discharge of a passively-charged capacitor through the injected mass will increase the plasma speed (see Fig.2). It is anticipated (because of the relative

RDA ADVANCED THRUSTER RESEARCH  
FAMILY OF THRUSTERS FROM PPT

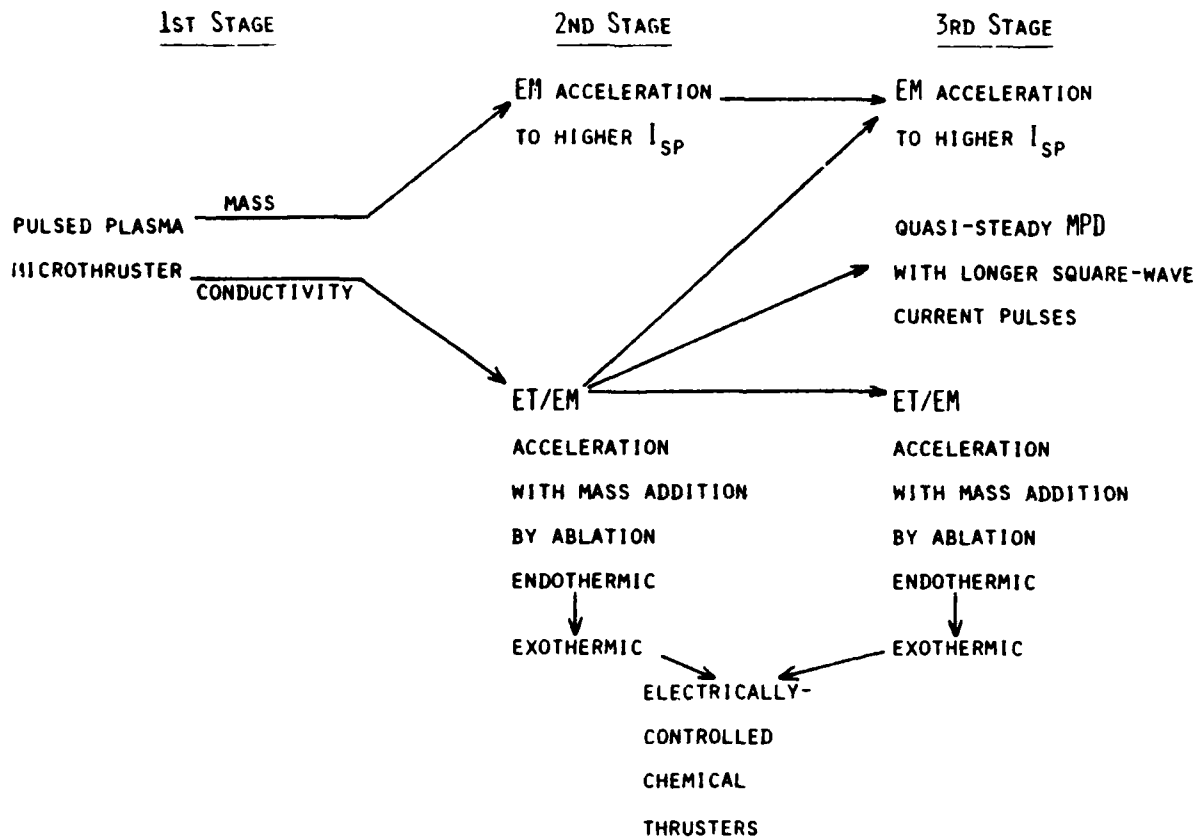


Figure 3

back EMF's) that most of the current flow, and therefore acceleration, will occur in the slower moving portions of the injected plasma, thereby improving the average  $I_{sp}$  (and improving the thruster efficiency).

The conductivity of the PPT exhaust can also be used to initiate a discharge over a relatively long surface of propellant in the second-stage, as depicted in Fig. 2. The second-stage discharge provides additional mass and energy without requiring modification of the PPT operation. The intrinsic performance of the second-stage should be better than the PPT because longer discharges provide improved impedance coupling to a passive-capacitor circuit, and also greater electromagnetic interaction with the flow. In fact, if the duration and level of the current are increased sufficiently, quasi-steady MPD operation should be possible with an ablatively-fed diffuse discharge.

The exhaust from the second-stage could be injected into a third-stage for either further electromagnetic acceleration or mass addition. The use of more than one additional stage would ameliorate the effects on total system performance of nonuniformities in the PPT exhaust. The second-stage could thus prepare a more useful plasma flow for the third-stage. Again, the power circuitry and fuel handling would be passive, so the entire system is controlled by the PPT. In particular, it should be possible to avoid high current switching and associated circuitry, which usually diminish the system performance (lower  $\eta$ , lower effective  $I_{sp}$  due to switch erosion) of pulsed plasma and quasi-steady MPD thrusters.

The choice of thruster arrangement, number of stages, electromagnetic vs electrothermal, coaxial vs rectangular, pulsed vs quasi-steady, etc., can be developed in response to mission needs. The entry level for operational use can be kept low by modest extension of the microthruster (with second-stages or millipound thrusters). Indeed, entry of the proposed family has already occurred in the form of the

microthruster. More demanding missions can be accomplished by increasing the current and pulsetime of the second (and/or third) stages. Operational experience can be shared by family members, providing greater confidence in design variations and allowing easier acceptance of new or more advanced systems. Evolution toward quasi-steady or even steady MPD arcjets should be possible, including extension to higher  $I_{sp}$  values if needed. (Presumably, the confidence gained with electric propulsion will also allow more ready acceptance of electrostatic techniques, if higher specific impulse and efficiency are required). For the lower specific impulse, higher thrust values needed to accomplish maneuvers quickly, chemical augmentation of electric thrusters may be possible by altering the average energy required to ablate propellant in the second or third-stages (using perhaps a mixture of endo- and exothermic materials as in plastic-bonded explosive). A change in thruster performance might then be accomplished simply by changing the fuel slab material. Use of an electrical discharge for ablation of chemically-active materials leads naturally to the notion of electrical control of chemical combustion in situations for which self-sustaining burning is not possible.

The development of a family of advanced thrusters based on the pulsed plasma microthruster comprises many possibilities and can include several on-going research programs, such as traditional millipound PPT efforts and various MPD studies (with minor alterations of approach). The present study explores aspects of multi-stage plasma thruster operation both theoretically and experimentally. The aim has been to provide an initial physical basis for the concept of utilizing a pulsed plasma microthruster in higher performance, multi-stage systems.

#### IV. THEORETICAL STUDIES

A second-stage of electromagnetic thruster could either accelerate the PPT exhaust plasma to higher (average) speed or utilize the PPT plasma to initiate an ablation arc. In this section, a plasma slug model is first used to examine the acceleration of PPT plasma by a second-stage thruster, normal or parallel to the original plasma velocity. A magneto-acoustic analysis is applied to indicate the processes involved in acceleration of a distributed plasma. The basic equations for convection and diffusion of magnetic field in a plasma are then inspected to discuss the operation of a second-stage in a quasi-steady, ablation mode.

Appendix A provides an elementary system analysis of pulsed plasma thrusters for orbit transfer indicating that pulsed operation with state-of-the-art capacitors can be adequate for such transfer missions. Substantial electrical power required by the payload and matching of a pulse forming network (PFN) of capacitors to the second-stage thruster are two conditions that must be satisfied. Appendix B displays a sample design of a second-stage thruster at 10 millipound average thrust level, utilizing a PFN matched to the impedancce of a quasi-steady ablation arc. An explanation of the so-called critical velocity in electromagnetic (self-field) thrusters is derived in Appendix C and indicates scaling of ablation-fed plasma thrusters with endo- or exo- thermic fuel slabs.

##### IV.1. ACCELERATION OF THE PPT PLASMA

The simplest form of multistage plasma propulsion consists of the PPT injecting a slug of plasma between two rail-electrodes that are connected to a charged capacitive power source. The capacitive source could be trickle-charged between PPT firings (in the manner of a photographic flash attachment) and could utilize capacitor elements of the same type used previously by microthrusters on actual long term space missions. If the PPT exhaust is directed in a perpendicular fashion across the rail gap (Fig. 4a), then the PPT merely provides

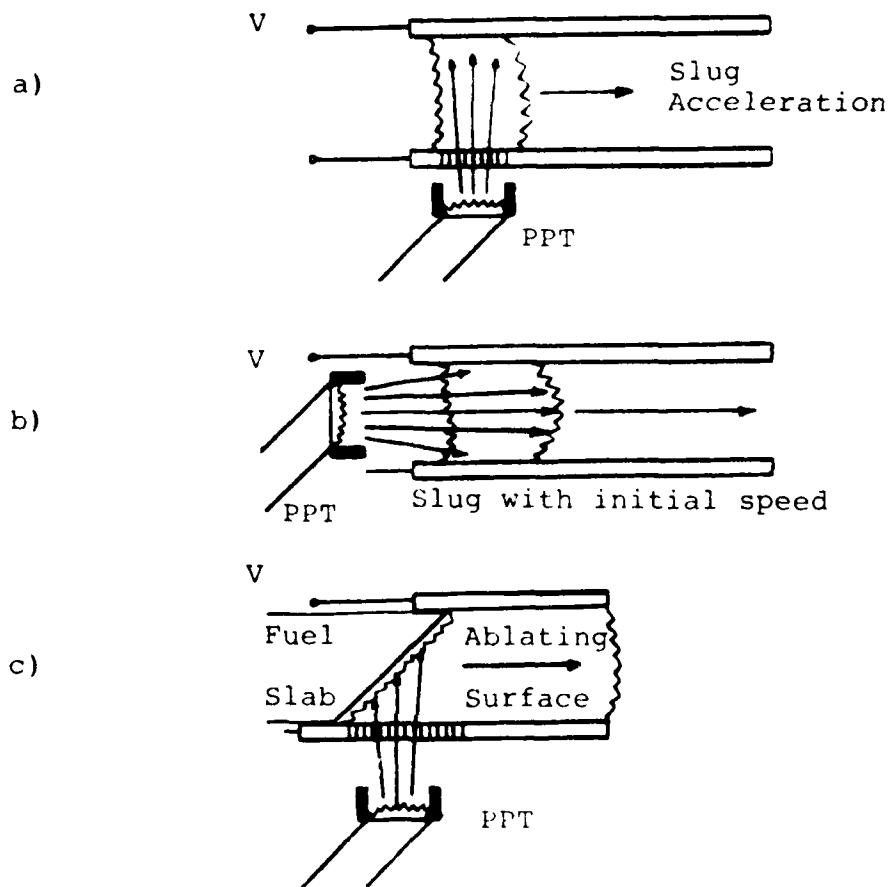


Fig 4 - Conceptual diagrams of plasma injection from PPT into second-stage thruster;

- a) injection across gap (eliminating PPT momentum);
- b) injection along electrodes to increase initial dynamic impedance;
- c) injection along second-stage insulator to initiate ablation for mass-addition.

mass (and a means of initiating current flow in the second-stage). The kinetic energy of the PPT exhaust is thus discounted in this example. Acceleration of the injected plasma along the rails is described by the usual set of lumped-circuit equations in which the electrical impedance of the accelerating plasma discharge is expressed as the rate of change of circuit inductance. By nondimensionalizing the equations, a single dimensionless parameter is obtained that determines the discharge dynamics:

$$\beta = \frac{E_0 F^2}{MZ^2}$$

where  $E_0$  = initial capacitor energy  
 $F$  = inductance change per unit length of plasma motion  
 $M$  = plasma slug mass  
 $Z = (L_0/C)^{1/2}$  = initial circuit impedance

In Fig. 5a, the kinetic efficiency,  $\eta = \frac{1}{2}mu^2 / CV_0^2$ , (for a desired exhaust speed  $u = \beta Z/F$  developed in the second-stage thruster) is seen to rise quickly as the dimensionless dynamic parameter  $\beta$  is increased to about  $\beta=3$ ; less rapid gains are achieved with higher values of  $\beta$ . (In these calculations, the dimensionless speed,  $\mu$ , achieves its peak value before the computation is ended).

If the PPT plasma is directed parallel to the rails, ( $\omega = \omega_0 \neq 0$ ) but spread across the rail gap to initiate current flow, as shown in Fig. 4b, then higher efficiencies are obtained because the moving plasma presents a higher initial (dynamic) impedance to the power supply. As shown in Fig. 5b, the kinetic efficiency  $\eta = \frac{1}{2}\beta(\omega^2 - \omega_0^2)$  can exceed 55%, while doubling the exhaust speed of the plasma slug ( $\omega_0 = .36$ ); the results shown are for  $\beta = 3$ . In dimensional variables, the simple slug acceleration model indicates that specific impulse values in the range of 1500 sec should be possible with system efficiencies in excess of 50%. Such values are not especially remarkable for electric propulsion techniques, but are encouraging as improvements on an existing space-tested thruster.

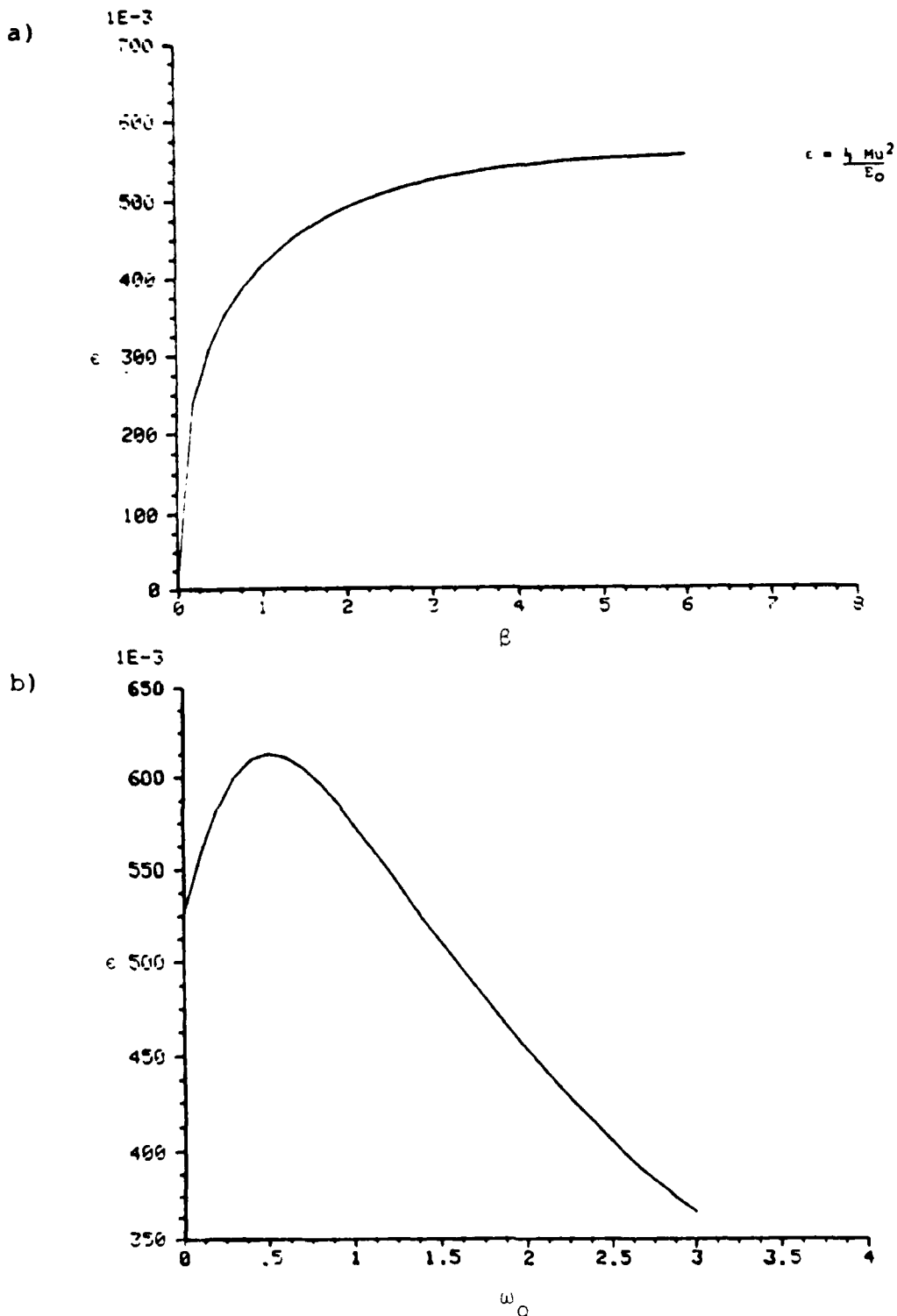


Fig 5 - Results from normalized lumped-circuit calculations:

- a) Efficiency of plasma slug acceleration versus dimensionless dynamic parameter  $\beta$  for case of zero initial streamwise motion.
- b) Efficiency of plasma slug acceleration versus initial normalized speed  $\omega_0 = u_0 F / 2S$ , for case of  $\beta=3$ . Flow speed doubles in the second-stage for  $\omega_0 = 0.36$ .

For near term missions (i.e., near earth vs outer planets), the optimum specific impulse based on available specific power values ( $\approx 30$  w/kg) will probably not exceed 2000 sec. The primary virtue of electric acceleration of the PPT exhaust plasma, therefore, is improved thrust efficiency. Such improvement has two aspects: 1) the increase in time-averaged dynamic impedance associated with acceleration of an initially moving plasma; and 2) the preferential acceleration of slower plasma that is emitted later in time by the PPT. The latter aspect recognizes that the PPT tends to provide two components of plasma. A fast component due to the PPT discharge is observed to exit the microthruster followed by a slower component associated with the continued ablation of the PPT fuel surface. The specific impulse is thus obtained as a temporal average over flow speeds that are higher and lower than optimum; it would be useful to reduce the velocity spread to achieve higher system efficiencies.

Acceleration of the distributed PPT plasma in the second-stage may be considered in terms of expansion of magnetized plasma. In Fig. 6, a semi-infinite plasma ( $x \leq 0$ ) is allowed to expand into a field-free vacuum ( $x \geq 0$ ). The plasma density may be calculated at any time and position from adiabatic expansion through a centered expansion fan. If the plasma resistivity is low, the magnetic flux will tend to convect with the plasma mass, so the spreading density gradient will correspond to a current distribution. At  $x=0$ , sonic conditions are maintained, so the downstream evolution of the plasma discharge can be modeled by the downstream expansion fan even if the semi-infinite magnetized plasma is replaced by a source of plasma from the PPT. (Resistive diffusion at the entrance to the second-stage is necessary to extract magnetic flux from the second-stage power circuit). The expansion fan analysis then indicates that about half the current will be carried in the downstream plasma discharge, while the remainder will flow near the inlet to the second-stage. If the injected flow density drops substantially, then a "contact surface"

EXPANSION OF SEMI-INFINITE MAGNETIZED PLASMA

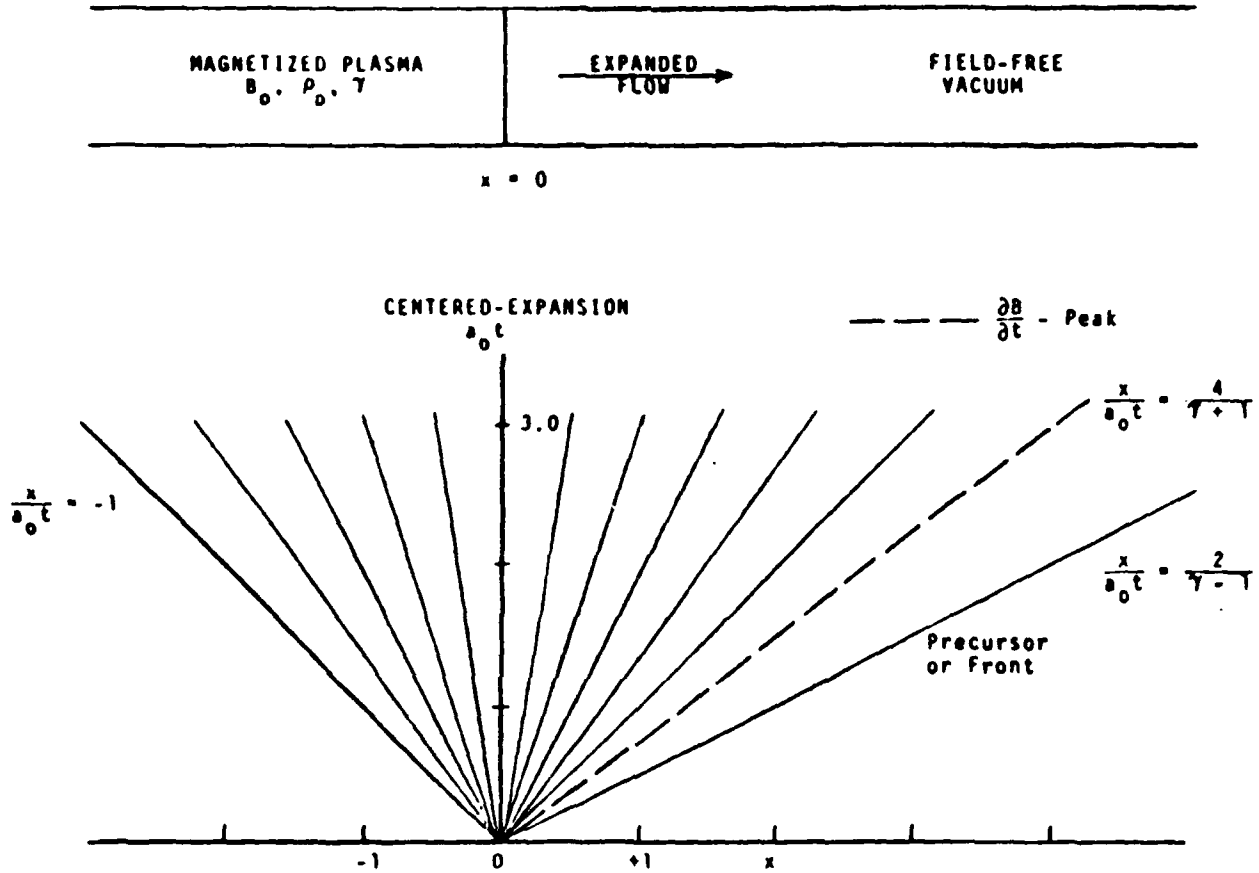


Fig 6 - Expansion of a semi-infinite magnetized plasma into a field-free vacuum. A centered expansion fan in the  $xt$ -diagram shows the spread of the current conduction region with time.

between the previously injected plasma and this low density flow will accelerate and sweep up the earlier plasma. For sufficient length of rails (about 15 times the effective "length" of the injected PPT plasma) a single plasma slug would exit the second-stage. The expansion and recollection of plasma in the second-stage is depicted in Fig. 7.

If the rail length is significantly less than the distance needed to recollect the plasma, then it would be more appropriate to consider magnetic diffusion (vs adiabatic expansion) as the mechanism establishing the discharge distribution. With proper insulation, acceleration of the plasma will cease slightly beyond the end of the rails and all the plasma injected into the second-stage should experience about the same change in momentum. To the extent that this momentum change is much greater than the initial momentum of the slower component of the PPT exhaust, the second-stage should exhibit a more uniform exhaust velocity and thereby achieve higher efficiency at a desired specific impulse level.

#### IV.2. GENERATION OF HIGHER THRUST AT FIXED $I_{sp}$

To obtain higher thrust at a fixed value of specific impulse, mass addition is necessary. A conceptually simple approach utilizes the PPT to initiate an arc over an insulating surface that then ablates due to the heat flux from the plasma discharge (Fig. 4c). The mass flow into the discharge thus depends on the local plasma current density, which in turn depends on the flow through the discharge. The physical situation resembles the flame zone over a solid propellant surface and will depend quantitatively on the details of the electrical resistivity and thermal conductivity of the flow as it changes from vapor to highly ionized plasma. Some qualitative insight, however, for purposes of the present discussion, may be obtained by examining the equations governing the discharge distribution downstream of the region of plasma formation.

The basic equation for the current distribution may be written as a balance of convection and diffusion of magnetic

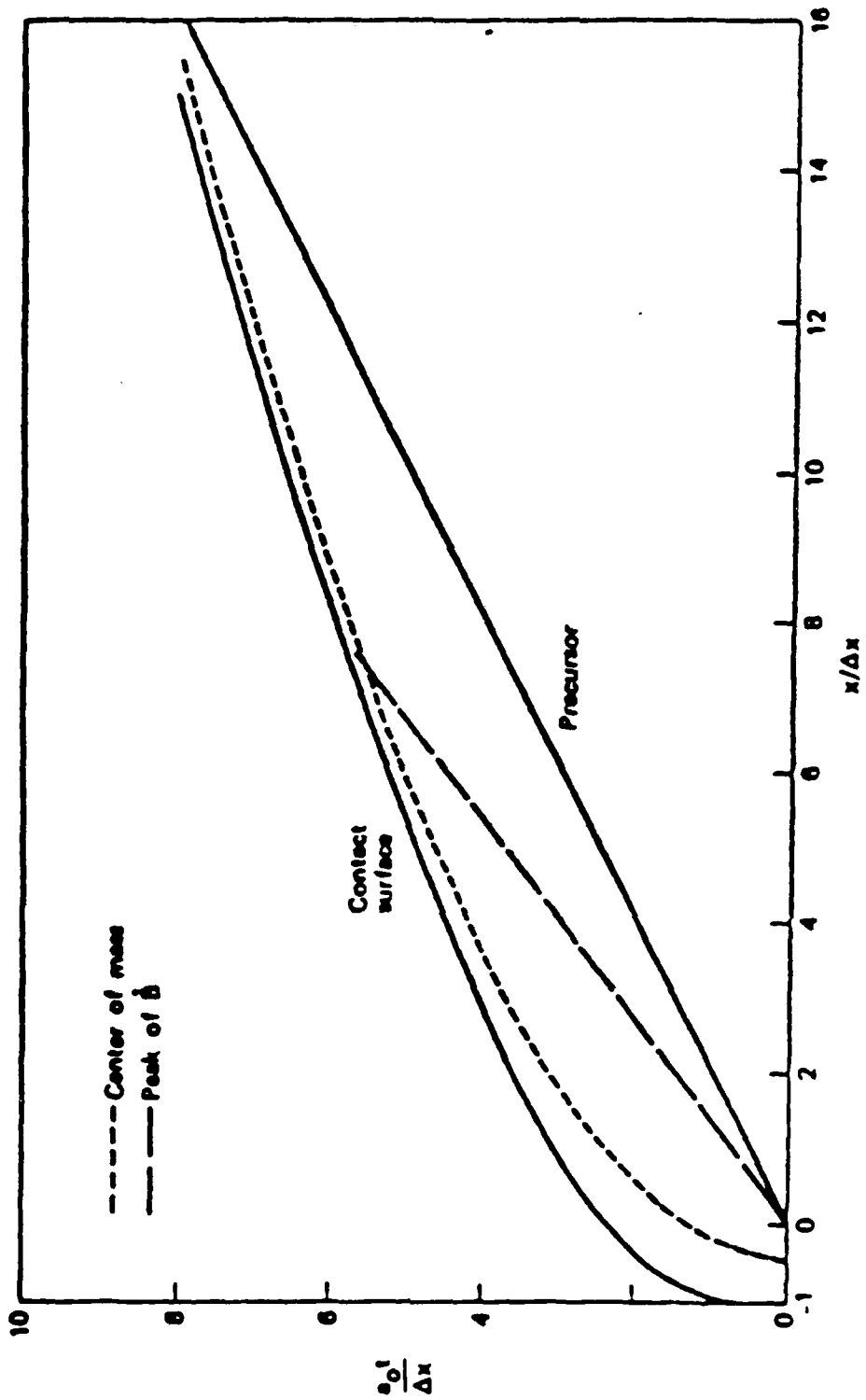


Fig 7 - Expansion and recollection of a plasma slab driven by a constant magnetic field. The contact surface indicates the boundary between high density plasma and vacuum if the PPT injection could stop abruptly.

field:

$$\frac{D_e}{Dt} \bar{B} = \frac{\eta^2 B}{\mu}$$

where the convective derivative is based on the electron fluid speed and a constant resistivity  $\eta$  downstream of the "flame zone" has been used for simplicity. If the plasma density is sufficiently high (electron current drift speed  $\ll$  plasma flow speed), then the plasma flow speed can be substituted for the electron fluid speed (thereby eliminating tensor current flow and electrode polarity effects from the MHD analysis); the electron pressure gradient term has already been neglected in the generalized Ohm's law used to obtain this equation.

In steady-state, and allowing only one dimension of spatial variation (i.e., streamwise), the convective vs diffusive balance becomes:

$$\frac{d}{dz} (uB) = \frac{\eta}{\mu} \frac{d^2 B}{dz^2}$$

where a uniform mass flow,  $F = \rho u$ , is invoked in order to eliminate mass density from the equation. In solving this equation, the streamwise location of the downstream boundary value ( $B=0$ ) is specified (or computed). If this location is specified, for a given upstream boundary condition ( $B=B_1$  at  $z=0$ , the downstream edge of the flame zone), then the current density corresponding to the current in the downstream region is determined. Higher flow velocity tends to convect magnetic flux downstream, increasing the current density near the  $B=0$  location at the expense of upstream positions ( $z > 0$ ). The current density, resistivity, and  $u \times B$  at  $z=0$  then provide the electric field that sets the volumetric heating rate of the plasma near the ablating surface. A portion of this heating supplies the energy needed for ablation and ionization, thereby scaling the mass flow rate. The higher the mass flow rate, the higher the flow speed for a given magnetic driving pressure and the greater the tendency to concentrate portions of the

current near the downstream  $B=0$  boundary location and in the flame zone. (Ablation driven by increased resistive heating in the "flame zone" can then compensate by raising the mass flow rate).

For a given maximum magnetic field (i.e., total current), placement of the  $B=0$  boundary further downstream lowers the current density and thereby lowers the dissipation that is providing mass flow to the plasma discharge. Thus, if the electrode rails of the second-stage are too long, ablation of the second-stage propellant slab may be insufficient during the current pulsetime from the power supply. Starvation of the discharge may then lead to electrode erosion (which is not the desired mechanism for mass addition). Such starvation may be mitigated by the continued influx of slower material from the PPT. The operation of the second-stage, however, would then resemble the expansion-acceleration mode discussed in the previous section.

Proper operation of the second-stage to provide mass addition therefore requires the minimum length of electrode rails consistent with the lateral dimension of the PPT exhaust. Since it is often the case that currents can be sustained in plasma flows that serve as extensions of physical (solid) electrodes, it is also important to avoid accelerating the PPT exhaust plasma out of the second-stage before ablation can replace the PPT mass flow. The rise time of current in the second-stage, therefore, should approximately match the pulsewidth of the PPT exhaust. Too short a risetime can lift off a current sheet of PPT plasma (plus initial ablation) from the insulator (in the manner sought for successful operation of some pulsed plasma guns). If the risetime is too long, however, the PPT plasma may splash downstream and severely shunt the insulator surface discharge.

## V. EXPERIMENTAL TESTS

Three experimental test series on multistage plasma propulsion have been conducted at the RDA Washington Research Laboratory. The first series corresponds to the case of flow acceleration in a second-stage with long electrode rails. The second series utilized short electrodes to achieve higher mass flow rates by ablation, and a third series shortened the electrodes further to concentrate current flow near the inlet. In all tests, an actual PPT from the Lincoln Laboratories production<sup>5</sup> for the LES-8/9 mission was used to inject plasma between electrodes connected to a charged pulse-forming network (PFN). The PFN is a 5-section voltage-fed synthetic transmission line with a 0.75 ohm characteristic impedance. The total stored energy is 22.5 kJ with the capacitors charged to 20 kV. The output pulse risetime (and decay time) is 8% of the design pulsewidth of 185  $\mu$ sec. At maximum operating voltage, the short circuit output current is 27 kA. A series ignitron switch is included in order to isolate the PFN from the experimental apparatus until the PPT plasma is ready to enter the second-stage; (this switch is for experimental convenience). In the present experiments, a series resistance of 0.75  $\Omega$  was included to prevent current reversal in the second stage.

The PPT and second-stage are stationed inside a 0.6 x 6 meter tubular stainless steel vacuum vessel that is evacuated to  $10^{-6}$  torr prior to thruster operation. In the vicinity of the thruster, the vessel is lined with Mylar. Several ports are available for probe feedthrough and optical diagnostic access. Figure 8 provides a sketch of the basic apparatus. The geometries of the second-stage systems are shown in Figures 9 and 10, long-rail and short-rail, respectively. The inlet-rail geometry is the same as the short rail system except that the electrodes are cut back to the inlet region and Pyrex sidewalls prevent the lateral expansion of flow in the thruster.

EXPERIMENTAL THRUSTER FACILITY

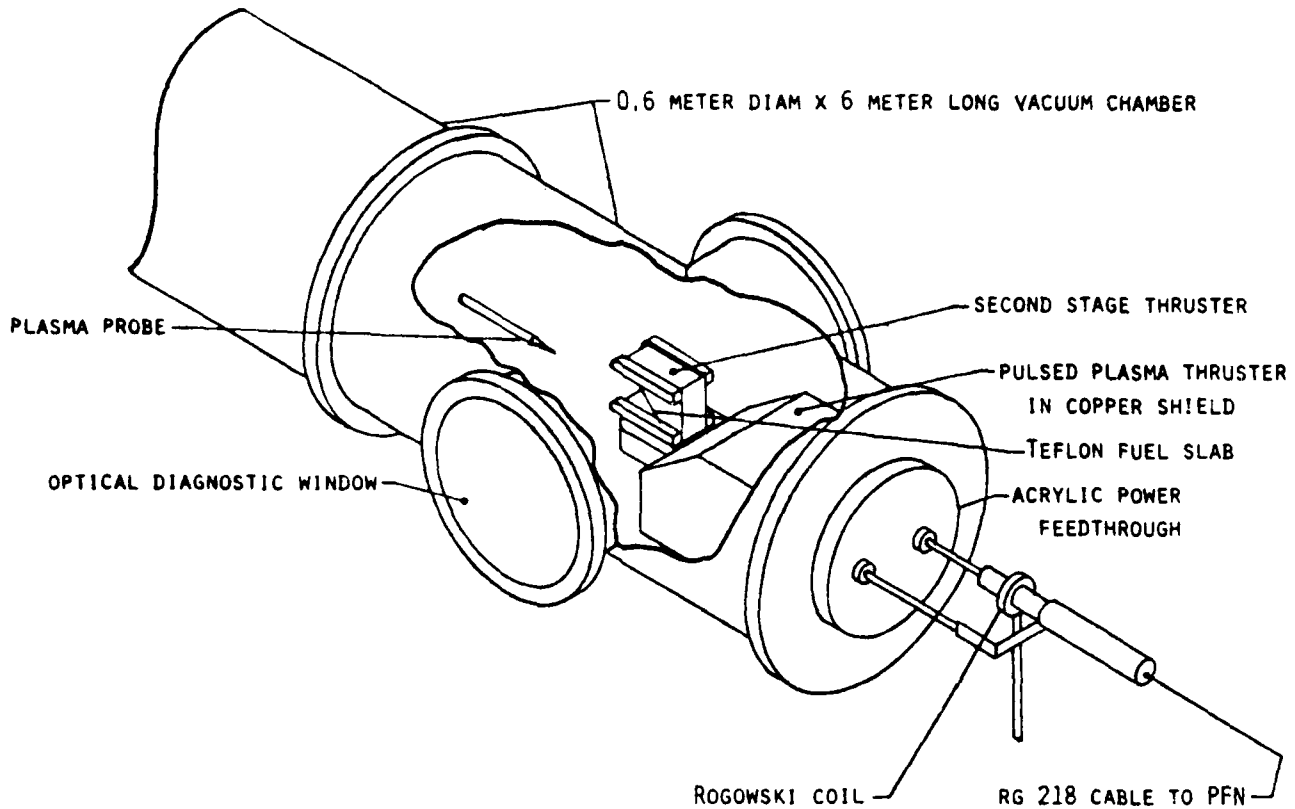


Fig 8 - Sectional view of Experimental Thruster Facility  
at the RDA Washington Research Laboratory.

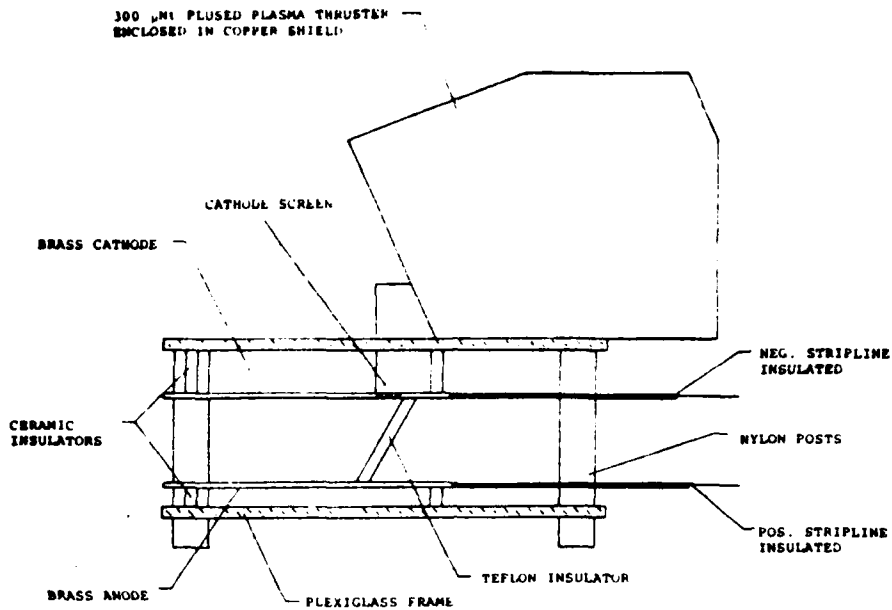


Fig 9 - Schematic diagram of long-rail experimental set-up.

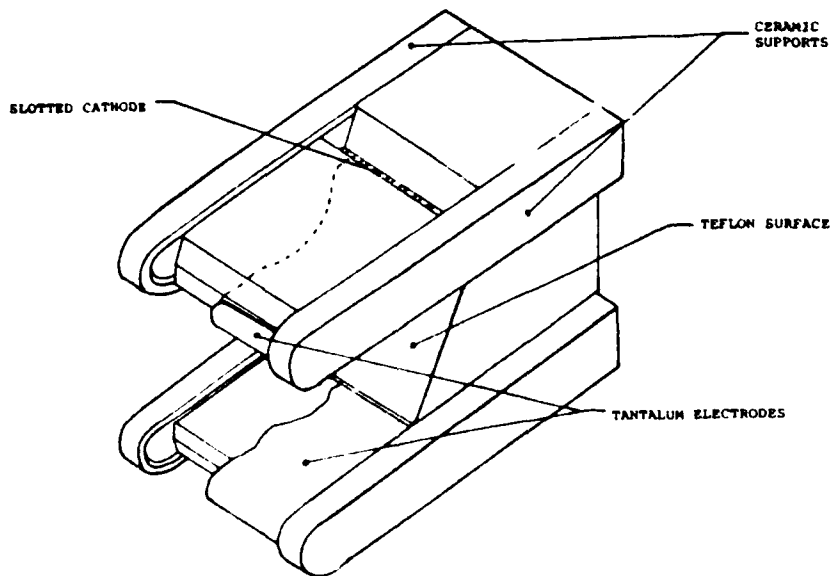


Fig 10 - Sectional view of second-stage in Short Rail Experiments. See Fig 8 for overall layout.

## V.1. LONG RAIL EXPERIMENTS

The long rail second-stage consisted of a brass anode and cathode each 6 mm thick. The anode was 28 cm long, the cathode was 23 cm long and the anode-cathode separation was 8.7 cm. All electrode edges were rounded with a 3 mm radius to reduce field enhancement. The effective width of the anode and cathode was 3.5 cm. This was maintained by two vertical acrylic dielectric channel walls that extended to the ends of the electrode system. Slots 1.5 mm wide cut into the upstream end of the cathode allowed plasma from the PPT to pass through the cathode and cross the face of a 6 mm thick Teflon insulator. The Teflon insulator was inclined at an angle of  $45^\circ$  with respect to the central axis of the electrode system. Plasma from the PPT was directed through a copper channel to the entry slots in the top of the cathode surface. A matrix of holes through the cathode beginning at 8 cm from the cathode-Teflon junction provided entry ports for magnetic B-probes into the plasma channel. Both anode and cathode rails were secured to acrylic sheet 1.27 cm thick by means of ceramic standoff insulators. The upper and lower acrylic sheets were in turn secured to each other by means of nylon rod insulators. Electrical connection to the anode and cathode was provided by braided copper straps covered with Tygon tubing. The tubing provided an insulating cover that prevented electrical breakdown between the vacuum chamber wall and the anode, and between anode and cathode.

Magnetic probes were constructed using 40 turns of #38 insulated copper wire wound on a 1 mm diameter mandrel. The coil leads were tightly twisted. The coil was then removed from the mandrel and impregnated with polystyrene. The coil was then cemented to an acrylic rod to insure constant orientation. The coil-tipped rod was then inserted into a 3 mm OD Pyrex sleeve, sealed at one end. The axis of the field-sensing coil is perpendicular to the axis of the Pyrex sleeve. For calibration, the rail gun was shorted at the muzzle end and the time resolved response of each probe was recorded along with the output of the capacitor bank/pulse-forming line.

In this way a matrix of in situ calibration factors was obtained for various probe locations. The short was removed and a set of time-resolved probe responses was obtained between 10 and 16 cm downstream from the inlet to the second-stage for probe channel penetrations of 1, 2, and 3 cm.

As the discharge current rose in the second-stage, after injection of the PPT plasma, magnetic field was detected rapidly at successive downstream locations of the magnetic probes. The plasma speed, indicated by time-of-arrival of signals at the probes, is approximately  $4 \times 10^4$  m/s. At 16  $\mu$ sec into the current pulse, over 80% of the total current is carried more than 15 cm downstream of the plasma inlet. At later times, however, this percentage drops to 70% ( $t=96 \mu$ sec) and 50% ( $t=156 \mu$ sec) indicating shunting of the current at positions closer to the inlet and second-stage Teflon insulator. Since interferometric measurements indicate that the PPT plasma pulse should be complete after about 20  $\mu$ sec, the gradual shifting of current upstream may be ascribed to ablation of the Teflon insulator. With the long-rail electrode system used in these tests, it therefore appears that the PPT plasma is rapidly swept downstream resulting initially in rather low current density near the second-stage insulator. Continued heating, however, gradually creates enough mass flow to shunt current, (but by this time the current pulse in the present experiments is nearly over). Time-resolved spectroscopy indicates that  $H\alpha$  intensity drops off more rapidly (after the first 20  $\mu$ sec of operation) than Zn I intensity, suggesting that electrode erosion may provide plasma for current conduction before sufficient ablation of the Teflon insulator occurs. (The  $H\alpha$  may be due to the surface contaminants blown out by operation with the initial PPT plasma). To achieve faster ablation of the second-stage insulator, a second series of experiments was performed with shorter electrode rails.

## V.2. SHORT RAIL EXPERIMENTS

The anode and cathode of the short rail second-stage were constructed from 0.8 mm thick tantalum sheet. Each electrode was 4 cm wide with the downstream end formed into a 6 mm diameter cylinder to reduce field enhancement. Field enhancement from the sides of the electrodes was reduced by burying the metal edges in ceramic support rails to a depth of 3 mm. The rail supports maintained the 4.6 cm anode-cathode electrode separation. A solid Teflon rod 5 cm square with one end face cut at  $45^\circ$  with respect to the central axis of the bar was located between the electrodes. The exposed (flat) lengths of the anode and cathode were 3 cm and 8 cm respectively. Slots 3 mm wide in the cathode electrode just above the Teflon rod provided entry ports for plasma from the PPT. Plasma reached these slots by passing through a conical chute in a Teflon block that secured the short rail second-stage to the PPT. Electrical connection to the second-stage electrodes was provided by braided copper conductors. Teflon tubing 6 mm in diameter slipped over the conductors prevented plasma discharges between the experiment chamber and the braided copper anode lead and between anode and cathode leads.

The goal of the short rail two-stage thruster experiments was higher thrust at approximately the same specific impulse as the PPT by means of additional mass ablation at the second stage insulator surface. The PPT was operated at 1875 V with a stored energy/shot of 30 J. As reported previously, this device ablates approximately 30  $\mu\text{g}$ /shot of Teflon ( $\text{CF}_2$ ) with a specific impulse of 1100 sec and an average impulse bit of 300  $\mu\text{nt-sec}$ .<sup>8</sup> Other work also indicates ion exit velocities of 2.8 cm/ $\mu\text{sec}$  and an exit plasma ionization level of 20-40%.<sup>10</sup>

The second stage was operated with a 5 kV charge on the PFN. Figure 11 shows a typical current trace and Figure 12 a typical voltage trace. The current risetime is 15  $\mu\text{sec}$  to 3-3.25 kA. The voltage rises initially to about 450 kV and then falls to about 250 V in approximately 50  $\mu\text{sec}$ .

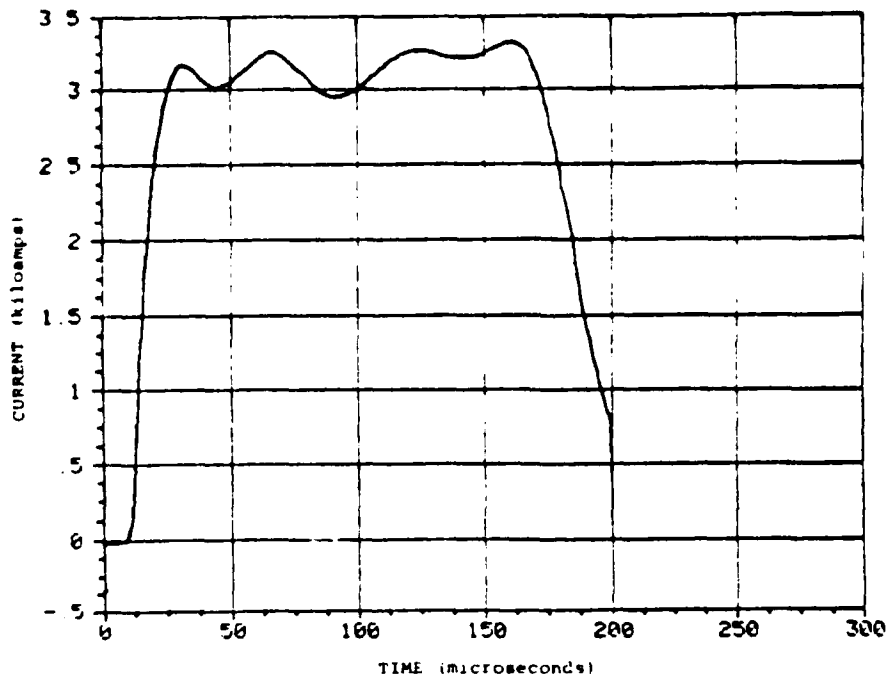


Fig 11 - Current vs time for the Short Rail Experiments with 5 kV on Pulse Forming Network.

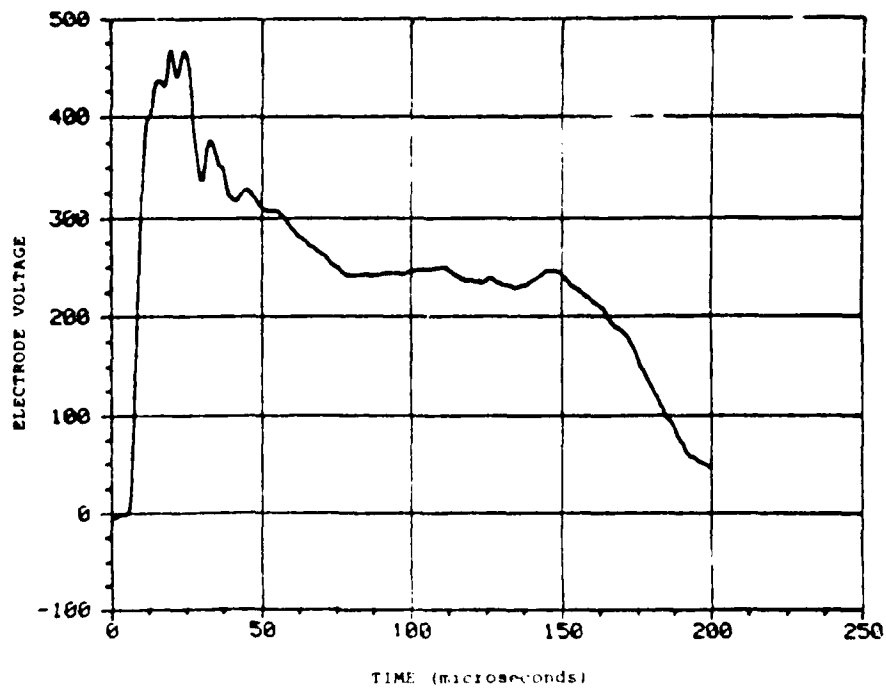


Fig 12 - Voltage vs Time for the Short Rail Experiments with  $V_0 = 5$  kV initial voltage on PFN.

Integration of the product of current and voltage indicates that the total energy deposited in the second stage after the PPT transient ( $t > 40 \mu\text{sec}$ ) was about 110 J.

In order to diagnose the short rail performance, two Langmuir probes were inserted 13 and 33 cm downstream of the end of the electrodes. The probes were made of tungsten wire 0.127 mm diameter and 1 mm long held in a sealed Pyrex tube. If the probe bias is sufficiently more negative than the floating potential (measured to be  $V_f = +35\text{V}$  with second-stage cathode grounded to the vacuum tank) the ion current is saturated at a level given (for  $T_i = T_e$ ) by<sup>12</sup>

$$I_{\text{ion, sat}} = S_p n_e \left( \frac{kT_e}{2\pi M} \right)^{1/2}$$

where  $S_p$  = probe area  
 $n_e$  = electron density  
 $T_e$  = electron temperature  
 $M$  = mass of the ions

With the two probes operating in ion current saturation, identifiable probe signatures during the middle and latter portions of the current pulse indicate a quasi-steady plasma stream velocity,  $u_s$ , of  $1.7\text{--}2.5 \times 10^4$  m/s. Figure 13 shows typical ion saturation currents for the two probes. The observed currents are continuous and relatively constant for the duration of the discharge indicating a constant ablation and acceleration of material out of the second stage.

The directed ion velocity (plasma stream velocity) may be on the order of the ion thermal speed which would imply that the ion current collected at the probe is strongly dependent upon the probe orientation in the plasma stream. To estimate the charged particle density, we therefore use the electron saturation current. If the probe bias is higher than the plasma space potential,  $V_s$ , the electron current collected is saturated and given by<sup>12</sup>

$$I_{e, \text{sat}} = S_p n_e \left( \frac{kT_e}{2\pi m_e} \right)^{1/2}$$

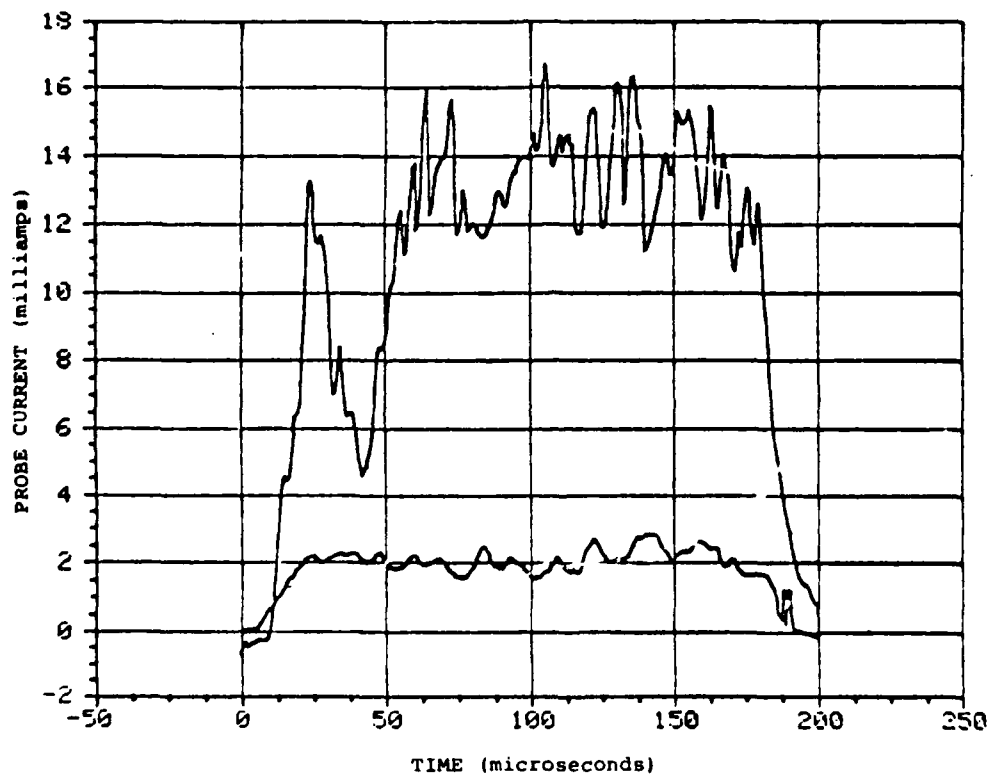


Fig 13 - Langmuir Probe Ion Saturation Current vs Time  
for the Short Rail Experiments  $V_0 = 5$  kV.  
 Upper Trace Probe 13 cm from Exit, Lower Trace  
 Probe 33 cm from Exit.

where  $m_e$  = mass of electron. Preliminary measurements of the electron temperature,  $T_e$ , of 2-8 eV imply an electron density at probe 1 of  $1.4-2.9 \times 10^{13}$  e/cm<sup>3</sup> and at probe 2 of  $3.5-7 \times 10^{12}$  e/cm<sup>3</sup>. (Previous measurement of the exit plasma temperature from the PPT assuming  $T_e=T_i$  indicated 7.2 eV<sup>10</sup>).

The total mass of material ejected by the second stage can be approximated by assuming  $T_e$  and the degree of ionization  $\alpha$  are constant at the probe positions. The lower current at the probe further downstream would then be due simply to expansion of the flow (i.e., thermal and angular spread of the exhaust jet). If a linear expansion is assumed from the exit plane of the second-stage, then the half-angle of the exhaust divergence is approximately 16°. (For Teflon,  $M = 16.7$ AMU, this divergence would correspond to a "thermal" energy of about 7 eV). The total mass flowing through the 18.4 cm<sup>2</sup> exit plane of the secondstage is then estimated to be 50-72  $\mu$ g, assuming  $T_e = 7$  eV,  $\alpha = 30\%$ , and  $u = 1.7-2.5 \times 10^4$  m/s. For the assumed speed, the impulse bit is therefore  $I = 0.85-1.8 \times 10^{-3}$  nt-sec, and the kinetic energy divided by input electrical energy is 6.6-20.5%.

It should be noted that the estimated impulse implies a driving pressure of about  $2.9-6.1 \times 10^3$  Pa, while the magnetic pressure in the second-stage should be about  $1-2 \times 10^3$  Pa. The energy for the flow may thus have substantial electrothermal contributions. In the present experiments, insulating channel walls on each side of the Teflon insulator were not used in order to force ablation only of the Teflon. The electrically-heated plasma may therefore be able to expand laterally as well as axially downstream. The total mass ablated per shot could then be up to three times larger than estimated from the Langmuir probe data. If the total mass flow could be channeled downstream by sidewalls (as in the PPT), then the kinetic efficiency of the second-stage might exceed 60%, with a total impulse in excess of  $5.4 \times 10^{-3}$  nt-sec.

### V.3. INLET-RAIL EXPERIMENTS

In the third series of tests, the lengths of the electrodes of the short rail system were decreased to 0.5 cm for the anode and 1.3 cm for the cathode (which has the inlet screen for the PPT plasma). The second-stage channel dimensions were maintained by substituting Teflon in the area formerly occupied by the electrodes; also, sidewalls of Pyrex were added to eliminate any lateral expansion of the plasma. The net effect of these changes is to concentrate the plasma and current density near the second-stage insulator and thereby to enhance ablation. Figure 14 displays the voltage and current record for a discharge with the PFN charged initially to  $V_0 = 15$  kV. The voltage trace is similar to the lower energy ( $V_0 = 5$  kV) test, but the current is now about 9.5 kA. Ion saturation current, measured 40 cm downstream of the thruster exit, is shown as a function of time for the same shot in Figure 15. Tests at lower initial voltage ( $V_0 = 5$  kV, 7 kV) indicate that the ion saturation current scales as the PFN energy, suggesting that the energy per particle is remaining constant, (which would be expected for processes involving ablation and ionization). At lower system energy, it was possible to obtain the full probe characteristic and thereby estimate the plasma temperature (and also obtain density measurement that is less sensitive to flow direction). From the slope of the probe current between floating and plasma potential, the temperature appears to be about 7 eV; the difference between floating and plasma potentials for the Teflon plasma indicates the same value. The divergence of the exhaust is also consistent with an ion temperature of 7eV. It appears then that plasma conditions are very similar to both the previous short rail tests and the earlier microthruster experiments by other groups. The difference in the present experimental series is the use of a current pulse that is maintained longer and at a constant level by means of a PFN.

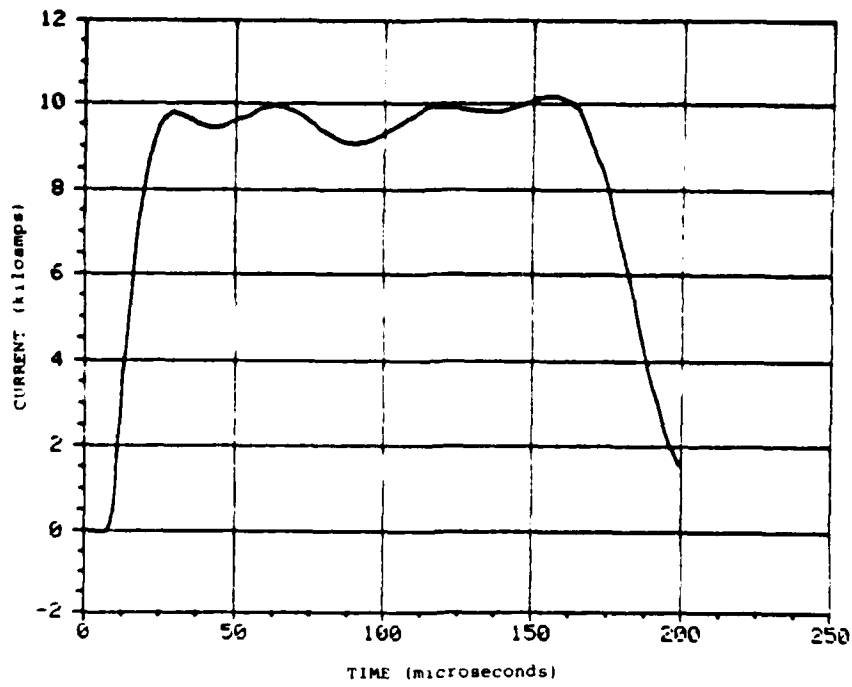


Fig 14a - Current vs Time for the Inlet-Rail Experiments with  $V_0 = 15$  kV.

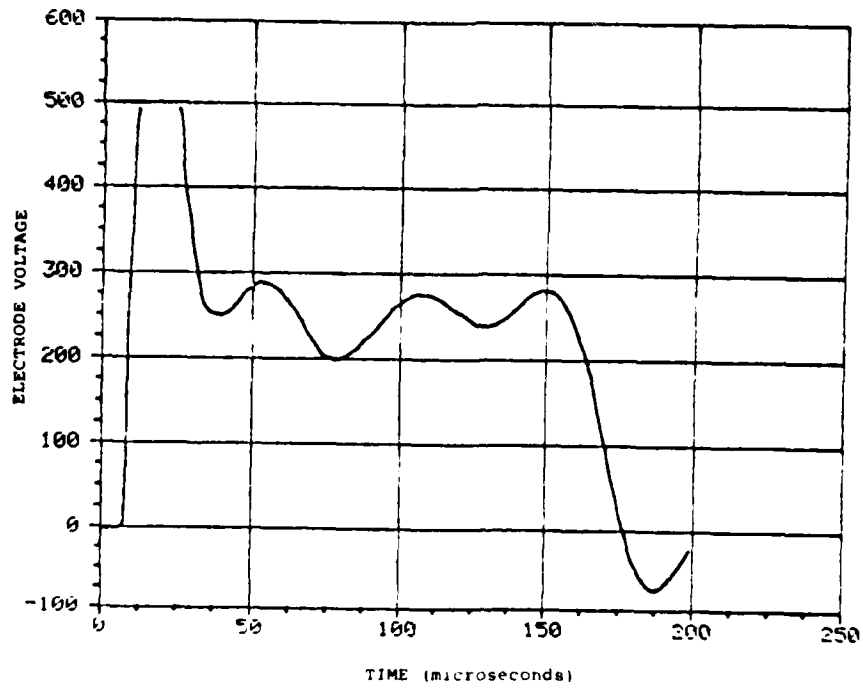


Fig 14b - Voltage vs Time for the Inlet-Rail Experiments with  $V_0 = 15$  kV.

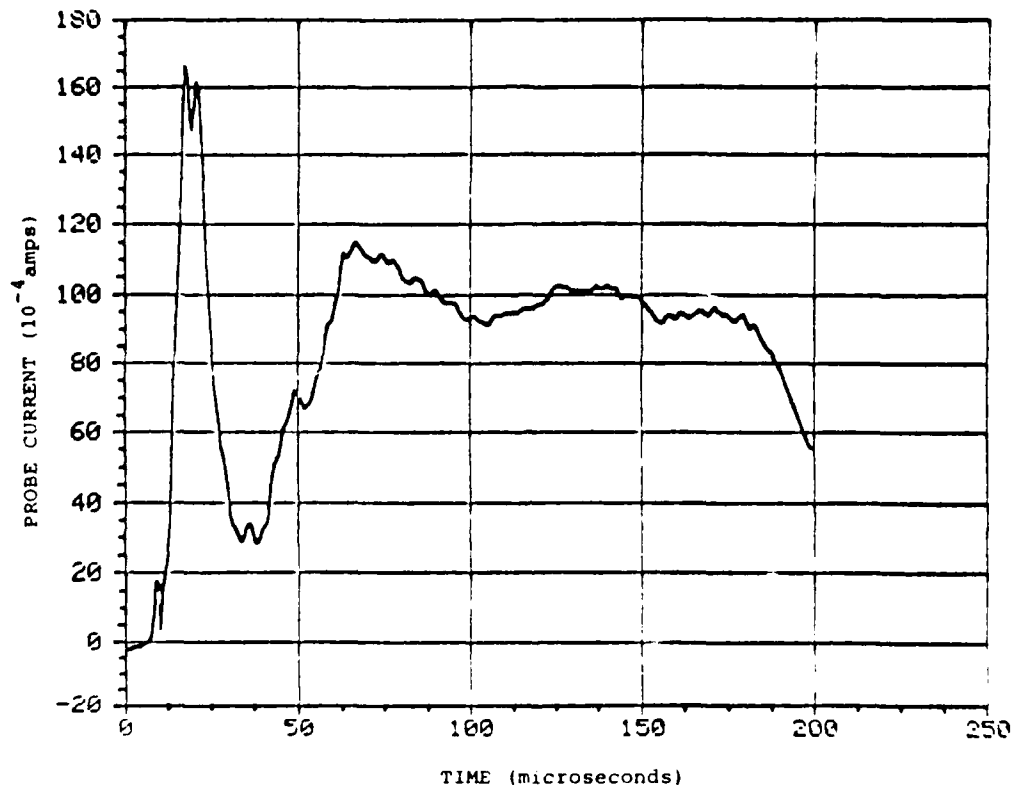


Fig 15 - Langmuir Probe Ion Saturation Current vs Time  
40 cm from Exit with  $V_0 = 15$  kV.

For the inlet-rail tests, at the highest initial  $V_0$ , the plasma density at the exit is estimated to be  $n_e = 1.3 \times 10^{15}$  e/cm<sup>3</sup>, which would imply an ablated mass of 500-730  $\mu$ g, if an ionization level  $\alpha = 0.3$  and flow speeds of  $1.7-2.5 \times 10^4$  m/s are again assumed. The efficiency of conversion of input electrical energy to flow kinetic energy would thus range from 23-72% depending on the values of  $\alpha$  and flow speed. Note that flow kinetic energy estimated using the charged particle density from probe data depends on the cube of the flow speed. Much better data are need to obtain an accurate measure of thruster performance.

## VI. CONCLUSIONS

A strategy for introducing electric propulsion into the U.S. inventory of techniques for near earth missions utilizes the space-operational pulsed plasma microthruster (PPT) in conjunction with additional stages of acceleration and/or mass addition. Such multistage plasma propulsion leads to a family of thrusters that would share operational experience as space-electrical power evolves. Theoretical considerations suggest possible modes of operation, including the transition from slug acceleration to surface ablation by varying the electrode dimensions. A series of experiments explored three thrusters, comprising pulsed acceleration of PPT plasma to  $4 \times 10^4$  m/s by a long second stage-thruster, and quasi-steady ablation of additional Teflon plasma in second-stages with short electrodes. The latter thrusters provide plasma speeds of  $1.7-2.5 \times 10^4$  m/s with nearly constant average particle fluxes for the duration of the current pulse (150  $\mu$ sec after the PPT transient).

The principal result suggested by the data from the short-rail and inlet-rail experiments is that a high temperature ablation arc can be maintained on a Teflon surface for the duration of the current pulse. This arc provides a high speed plasma flow that achieves quasi-steady conditions (during the 150  $\mu$ sec pulse of the present experiments, at least) with a specific impulse in the range of 2000 sec. The voltage drop across the second-stage ( $\sim 200$  V) is significantly larger than the cathode fall ( $\sim 35$  V), so the ablation arc should be rather efficient in converting electrical energy to flow energy.

Since the impulse per shot is proportional to the duration of the current pulse, there should be considerable flexibility in matching a second-stage thruster (triggered by a PPT) to a variety of mission requirements and power supply limitations. For low power missions, such as station-keeping, the multi-stage system should perform like present microthrusters that

have already seen application in space, but the multistage devices can have higher thrust. As higher levels of space prime-power become available, the current pulse duration can be extended to match the available power at the same repetition rate with the same type of capacitor components used in the present PPT (so lifetime and specific power of the pulsed source should not be a problem). If still higher powers are available, higher current operation would allow magnetoplasma-dynamic processes to become more important, so the second-stage could become a quasi-steady MPD arcjet (without propellant valves); alternatively, steady MPD or thermal arcjet operation would be possible. In all cases, end feeding of propellant bars, as in the PPT, allows the geometry to be preserved during long term operation. The present preliminary work on multistage plasma propulsion thus indicates that a single thruster arrangement could be coupled to progressively higher powers simply by adjusting a single extensive variable (the pulsewidth), maintaining the basic physical processes of the thruster as space experience is accumulated.

## VII. REFERENCES

1. Stuhlinger, E., Ion Propulsion for Space Flight, McGraw-Hill, New York, 1964, p. viii.
2. Jahn, R.G., Physics of Electric Propulsion, McGraw-Hill, New York, 1968.
3. Kaufman, H.R., and Robinson, R.S., "Electric Thruster Performance for Orbit Raising and Maneuvering", in Progress in Astronautics and Aeronautics.
4. Clark, K.E., and Jahn, R.G., "Quasi-steady Plasma Acceleration", AIAA Journal, Vol. 8, 1970, p. 216.
5. Vondra, R.J., and Thomassen, K.I., "Flight Qualified Pulsed Electric Thruster for Satellite Control", Journal of Space-craft and Rockets, Vol. 11, 1974, p. 613.
6. Stuhlinger, E., Ibid., Chapter 4.
7. Vondra, R.J., Thomassen, K., and Solbes, A., "Analysis of Solid Teflon Pulsed Plasma Thruster", Journal of Space-craft and Rockets, Vol. 1, Dec 1970, pp. 1402-1406.
8. Thomassen, K., and Vondra, R.J., "Exhaust Velocity Studies of a Solid Teflon Pulsed Plasma Thruster", Journal of Space-craft and Rockets, Vol. 9, Jan 1972, pp. 61-64.
9. Solbes, A., and Vondra, R.J., "Performance Study of a Solid Fuel Pulsed Plasma Electric Microthruster", Journal of Spacecraft and Rockets, Vol. 10, Jun 1973, pp. 406-410.
10. Thomassen, K., and Tong, D., "Interferometric Density Measurements in the Arc of a Pulsed Plasma Thruster", Journal of Spacecraft and Rockets, Vol. 10, Mar 1973, pp. 163-164.
11. Palumbo, D.J., "Solid Propellant Plasma Propulsion System Development for N-S Stationkeeping", in Progress in Astronautics and Aeronautics, Vol. 79, 1981, p. 652.
12. Huddleston, R.L., and Leonard, S.L., Plasma Diagnostic Techniques, Academic Press, New York, 1965.

APPENDIX A

PULSED PLASMA THRUSTERS FOR ORBIT TRANSFER

## PULSED PLASMA THRUSTERS FOR ORBIT TRANSFER

### Abstract

Pulsed plasma thrusters have previously been used for satellite station-keeping. The present paper briefly examines the application of the technology developed for such thrusters to orbit transfer (LEO-to-GEO). Simple estimates indicate that capacitor energy density and lifetime are sufficient to allow operation at specific impulse levels of about 2000 sec, so substantial fractions of the initial system mass can be delivered usefully to geosynchronous orbit. Recent experiments suggest that thruster operation in an electrothermal/electromagnetic ablation mode can be extended to arbitrary current pulsewidths using pulseforming networks. Thruster physics and operating performance can therefore be maintained as missions evolve, with increasing levels of space electric power, from low power pulsed plasma thrusters to quasi-steady or steady arcjets. Such evolution allows the accumulation of space flight experience and confidence critical for practical acceptance of electric propulsion.

### Introduction

The use of electric propulsion for near earth missions has recently received increased attention with the recognition of possible long-duration missions involving payloads that require substantial levels of electrical power. If most of the mass of the power supply (including heat rejection) can be ascribed to the mission payload, then the optimum exhaust velocity can increase substantially above levels accessible with chemical thrusters. From classic mission analyses for electric propulsion<sup>A-1</sup>, the optimum exhaust speed is given by:

$$u = (k \eta \epsilon)^{1/2}$$

where  $k = 1-2$  depending on the ratio of  $u$  to the necessary velocity increment  $\Delta v$ ;  $\eta$  is the efficiency of thrust power from total power,  $\epsilon$  is the specific power associated only with the electric propulsion system and  $t$  is the mission time.

If the total power system has a specific power of 30 w/kg, for example, but 80 percent of this system is needed by the mission, then  $\alpha = 150$  w/kg. A thirty-day mission (with  $k=2$  and  $\epsilon=0.5$ ) would then have an optimum specific impulse of 2000 sec.

There are several electric propulsion concepts that could satisfy this specific impulse requirement<sup>A-2</sup>. The present paper discusses some aspects of a particular approach that is based on a system that has already performed successfully (albeit modestly) on long term space missions<sup>A-3</sup>, the pulsed plasma microthruster or PPT. The principal interest is the introduction of electrical propulsion in a manner that can evolve as electrical power levels increase, drawing on actual flight experience, while maintaining the physical processes in the thruster. Such introduction would benefit from experience with the PPT design<sup>A-4</sup>. That is, optimization of thruster performance can be sacrificed to system simplicity in order to match available power supplies and minimize risk. For example, the PPT uses a Teflon fuel block fed into the electrode region by a negator spring, and thus avoids repetitive valve operation and cryogenic fuel storage. Furthermore, arc discharges tend to operate at voltages that are independent of the charging voltage of the current source. The energy from a pulsed plasma thruster might vary slightly from shot to shot, but the requirement for voltage regulation of the power supply is much less severe than for other types of electric thruster.

The present paper reviews some aspects of mission performance using pulsed plasma thrusters. Recent experimental work<sup>A-5</sup> then suggests the possibility of a single thruster that could match increasing space-electric power levels.

#### Pulsed Specific Power

As noted in the introduction, the optimum exhaust speed depends on the product of specific power  $\alpha$  and mission time  $\tau$ . For pulsed plasma thrusters, it is reasonable to expect that the specific mass,  $\alpha^{-1}$ , will be dominated by the energy storage system. Such approximation is based on the recognition that

most of the steady power components of the total electrical system (e.g., prime power source, heat rejection elements) may be used in performance of the spacecraft mission. The equivalent specific power of an energy storage component may be defined as the product of its specific energy  $E$  and the repetition rate  $f$ :

$$\alpha = Ef$$

The product  $\alpha T$  is then merely:

$$\alpha T = EN$$

where  $N$  is the number of shots in the course of the mission. The limiting value of  $N$  is the lifetime of the component.

The principal concern for pulsed plasma systems will probably be the capacitors used to accumulate energy from the power system between thruster firings. For the pulsed plasma microthruster<sup>A-3</sup>, a capacitor was developed with a product of specific energy density and lifetime that extrapolated to  $EN = 1.1 \times 10^9$  J/kg. This would be reasonably in excess of the  $\alpha T$  used in the Introduction ( $\alpha T = 3.9 \times 10^8$  J/kg). Since the pulsed plasma microthruster has operated on actual missions, firing once a second during the course of a year, it appears that a critical component for pulsed plasma thrusters applied to orbit raising has already been developed. (More recently, capacitors for quasi-steady MPD arcjet thrusters have been reported<sup>A-6</sup> with  $E \approx 80$  J/kg and  $N > 10^7$ ).

#### Orbit Transfer LEO-to-GEO

It is useful to make some simple estimates of the mission capability that could be achieved merely by extrapolating PPT technology. The characteristic velocity increment needed for a LEO-to-GEO transfer is quoted<sup>A-7</sup> as  $\Delta v = 6000$  m/s. At a specific impulse of 2000 sec, the fraction of initial mass delivered to GEO is then:

$$\frac{M_f}{M_o} = e^{-\Delta v / I_{sp} g_o} = 0.74$$

The fractional mass of the propellant utilized is therefore:

$$\frac{M_p}{M_o} = 1 - \frac{M_f}{M_o} = 0.26$$

To achieve this level of propellant utilization by ablation in the pulsed plasma thruster, requires accumulation of ablation per capacitor discharge over the N shots during the mission. Experimentally, the rate of ablation is approximately 2.5  $\mu\text{g}/\text{J}$  per shot. The total capacitor mass is then:

$$\begin{aligned} M_{\text{cap}} &= \frac{M_p}{(2.5 \mu\text{g}/\text{J}) EN} \\ &= 0.1 M_o \end{aligned}$$

The mass of the payload (including the power source needed for both mission and propulsion tasks) is obtained by subtracting this capacitor mass from the delivered mass:

$$M_\ell = M_f - M_{\text{cap}} = 0.64 M_o$$

This result overestimates  $M_\ell$  by neglecting the mass of the thruster itself and other power conditioning required only by the propulsion system. A more exact calculation, however, requires a more detailed specification of the mission; in particular, the power conditioning for propulsion could benefit from voltages higher than the 28 V generally available to meet mission needs. That is, it may be possible to access the spacecraft power utilizing mission-related power conditioning, rather than merely accepting bus voltage levels. The main point of the present calculation is that substantial fractions of the mass at LEO can be delivered usefully to GEO with technology that is based on present capabilities.

#### Variation of Mission Requirements

If the capacitor lifetime depends only on the number of shots, then higher power missions (shorter transfer times) can

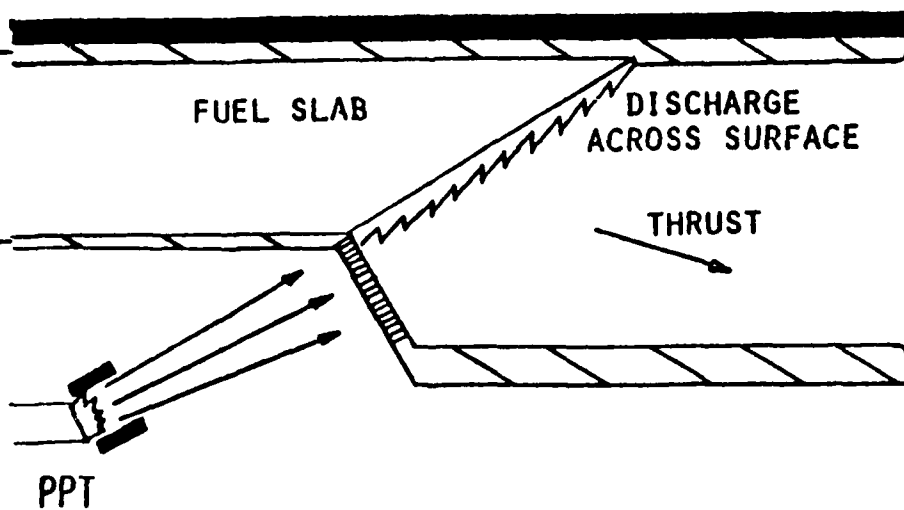
be accomplished simply with higher repetition rates and/or longer current pulsewidths. That is, to the extent that the capacitors dominate the specific mass, the  $QI$ -product is maintained independent of  $I$  ( $QI = EN = \text{constant}$ ). The optimum specific impulse is also constant, so the delivered mass fraction depends only on the necessary  $\Delta v$  for the mission.

The size of the capacitor supply will increase with the size of the mission payload. For fixed transfer time, the average thrust required will also increase with payload mass. Since the number of shots  $N$  is set by the capacitor lifetime, the repetition rate is fixed in this case and the current pulsewidth increases with the mass of capacitors.

Recent experiments<sup>A-5</sup> indicate that plasma flow conditions similar to the PPT flow can be maintained for the length of the current pulse in a two stage thruster system. This system uses an actual microthruster (for the LES 8/9 mission) to initiate current flow in an ablation thruster driven by a pulse forming network. The arrangement is shown conceptually in Fig. A-1. Data suggest that quasi-steady exhaust speeds of  $1.7\text{-}2.5 \times 10^4$  m/s are achieved after the initial microthruster plasma clears the second-stage, for the remainder of the flat-topped current pulse ( $\sim 160$   $\mu\text{sec}$ ). The impulse per discharge appears to scale with system energy over an order of magnitude variation in PFN energy. Preliminary estimates of kinetic efficiency divided by input electrical energy indicate an efficiency of 23-72 percent. It would thus appear possible to vary current pulsewidth and maintain useful efficiency at a specific impulse of about 2000 sec.

#### Concluding Remarks

From earlier work on pulsed plasma microthrusters and recent efforts involving extended, constant current waveforms, the technology for a family of pulsed plasma thrusters could reasonably be applied to near-earth missions, including orbit transfer. Such a family would allow electric propulsion to be introduced into the U.S. inventory in an evolutionary manner



ET/EM ACCELERATION  
WITH MASS ADDITION  
BY ABLATION

Fig A-1 - Conceptual schematic of the use of a PPT with a second-stage thruster to obtain higher thrust by ablation of a fuel slab. Experiments with this basic geometry are reported in ref 5.

as space-electrical power becomes available<sup>A-8</sup>. In particular, it appears that an ablation arc on a Teflon slab, with combined electrothermal and electromagnetic contributions to thrust, provides an adequate propulsion mechanism in the  $I_{sp}$  range of 2000 sec. Such an arc can be operated in both pulsed and quasi-steady conditions indicating that thruster physics can be maintained as prime-power levels extend from kilowatts to megawatts. Operational experience could thus be shared within this family of thrusters, providing confidence in performance as higher power missions are defined. Such confidence is probably critical to the practical introduction of electric propulsion in U.S. space missions of the next few decades.

#### References

- A-1. Stuhlinger, E., Ion Propulsion for Space Flight, McGraw-Hill, New York, 1964. Chapter 4.
- A-2. Caveny, L.H., ed., Orbit-Raising and Maneuvering Propulsion: Research Status and Needs, Progress in Astronautics and Aeronautics, Vol 89. AIAA, New York, 1984.
- A-3. Vondra, R.J., and Thomassen, K.I., "Flight Qualified Pulsed Electric Thruster for Satellite Control", Journal of Spacecraft and Rockets, Vol 11, 1974, p. 613.
- A-4. Guman, W.J., Vondra, R.J., and Thomassen, K.I., "Pulsed Plasma Propulsion System Studies", AIAA Paper No. 70-1148, 1970.
- A-5. Turchi, P.J., Boyer, C.N., and Davis, J.F., "Multi-Stage Plasma Propulsion", 17th International Electric Propulsion Conference, Tokyo, 1984. IEPC Paper No. 84-51.
- A-6. Harada, H., Gohnai, T., Yoshida, T., Obara, H., Kuriki, K., "Metallized Plastic Film Capacitor for MPD Thruster", *ibid.* IEPC Paper No. 84-27.
- A-7. Poeschel, R.L., and Hyman, J., "A Comparison of Electric Propulsion Technologies for Orbit Transfer", Ref. 2, p. 203.
- A-8. Turchi, P.J., "An Electric Propulsion Development Strategy Based on the Pulsed Plasma Microthruster", AIAA Paper No. 82-1901, 1982.

APPENDIX B

SAMPLE DESIGN OF A TWO-STAGE THRUSTER

## SAMPLE DESIGN OF A TWO-STAGE THRUSTER

An example of a possible two-stage thruster based on the pulsed plasma microthruster is shown schematically in Fig. B-1. The conceptual design goal is 10 mlb average thrust at a specific impulse of about 1000 sec. Total operation of the thruster for one year is desired. Values of the assumed performance (simply scaled from the microthruster operation) and derived thruster parameters are given in Table B-I. Briefly, the two-sided microthruster package used for station-keeping on the LES 8/9 communications satellites is inserted in the space between a pair of fuel slabs that each extend between electrodes connected to a trickle-charged transmission line. The microthruster can be fired by command logic to create a plasma stream along the surface of either fuel slab in the second-stage. Closure of the interelectrode gap by the plasma flow across the fuel slab allows the transmission line to discharge. The transmission line consists of a LC-ladder that is folded so either side of second-stage can discharge the line; at the electrical midpoint of the line (not shown) a steady power supply is connected. The storage capacitors are assumed to be the same as used in the microthruster, with a value of 80 J/can at 3000 volts. The inductance of the line is adjusted to match the load impedance approximately to the discharge impedance. The line should therefore discharge with high efficiency in 26  $\mu$ sec at a current of approximately 40kA. (Note that these pulsetime and constant current values are approaching quasi-steady MFD operation, c. 1969). Rather fortuitously, the folded line and microthruster fit under the fuel slabs for a thruster system length of about 1.7 meters. The fuel length is based on one year operation at a total repetition rate of 1 Hz. The average electrical power required at this rate is 1.7 kwatt. Such power levels indicate that a 10 mlb, 1000 sec thruster is not a trivial capability; the total mission impulse is equivalent to 10,000 lbs for 30 seconds.

The thrust efficiency based on the average exhaust speed and impulse bit for the microthruster (upgraded by a factor of

RDA ADVANCED THRUSTER RESEARCH

SCHEMATIC OF ELECTROMAGNETIC AFTERBURNER

SCALED FOR 10 MLB-S/SEC  
AVERAGE THRUST FOR ONE YEAR

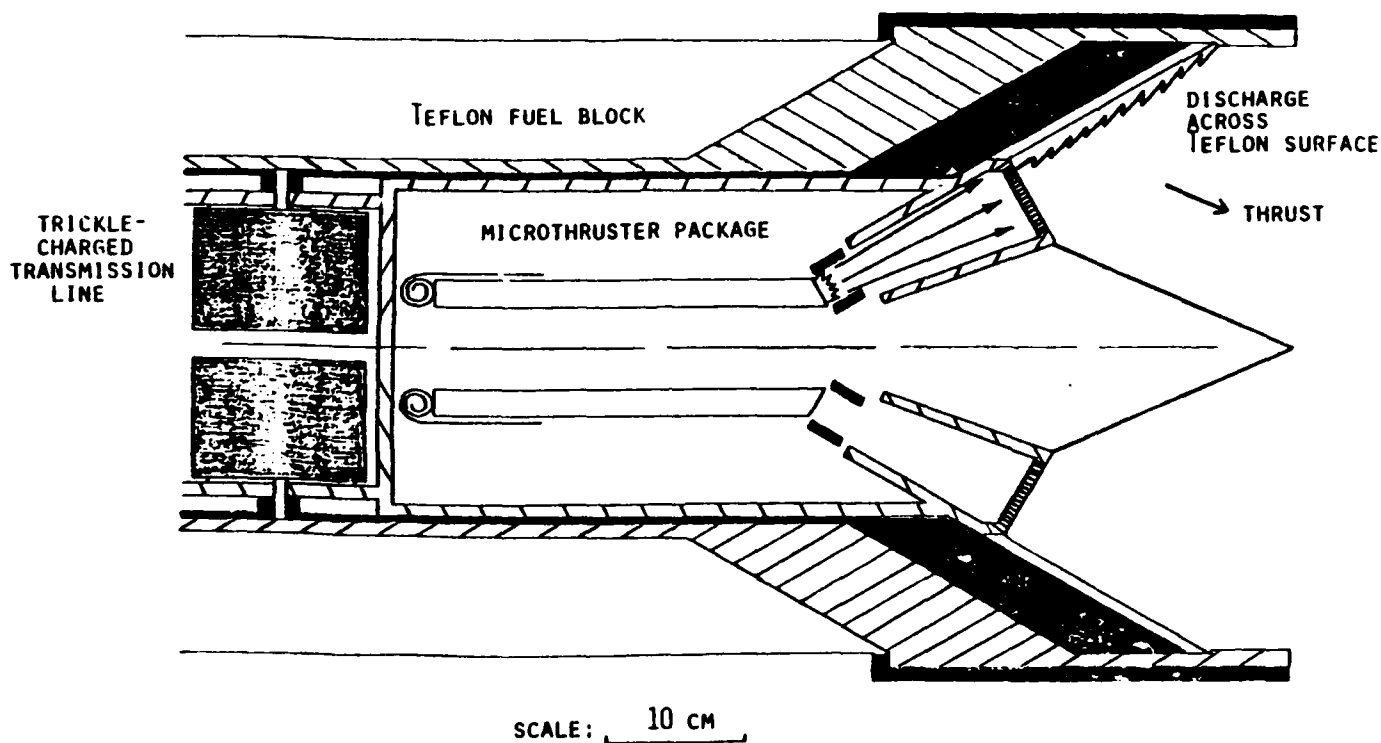


Figure B-1

two in thrust/watt from experience with millipound engines<sup>B-1</sup>) is  $\eta = 12.5\%$ . For pulsed plasma thrusters, the product  $\alpha_T$  in the formula for optimum exhaust speed converts to the joules/kg of the storage system multiplied by the number of firings per mission. If the tested lifetime of the capacitors<sup>B-2</sup> ( $>3.7 \times 10^6$  shots) is combined with their specific energy (41 J/kg), then the upper limit on  $\alpha_T$  is  $1.5 \times 10^8$  J/kg. With  $\eta = 12.5\%$ , and  $k = 1.5$ , the optimum specific impulse is 544 sec. The extrapolated capacitor life<sup>B-2</sup> with lower energy density capacitors would give  $\alpha_T = 1.1 \times 10^9$  J/kg, corresponding to an optimum  $I_{sp}$  of 1465 sec. The design goal of 1000 sec assumed in the sample calculation is therefore probably reasonable. (Note that at 1 Hz, the specific power associated with the capacitors is 41 w/kg, which is significantly less than values predicted for future space-power sources,  $\sim 100$  w/kg, so the capacitor weight should dominate the calculation of  $\alpha_T$ ).

Table B-I

Specifications:

Average Thrust	10 mlb-sec/sec
Operating frequency	1 Hz (0.5 Hz per side)
Total Operation	1 year ( $3.15 \times 10^7$ shots)

Assumed Performance:

Thrust/watt	5.9 mlb/w (twice 2.95 mlb/w for microthruster)
Ablated mass/joule	2.5 $\mu$ g/joule
Storage Capacitor	30 joule/can @3000 volts (same size as thruster can)

Derived Values:

Stored Energy	1.7 kjoule (22 capacitors)
Stored Mass	66.9 kg per side
Fuel Volume	$2.5 \times 10^4$ cm <sup>3</sup> per side
Fuel Slab Dimensions	Length 150 cm
	Width 18.5 cm
	Thickness 9.1 cm
Approximate Current	40kA
Approximate Pulselength	25 $\mu$ sec

Bibliography

- B-1. R.J. Vondra, private communication.
- B-2. R.J. Vondra, and K.I. Thomassen, "Flight Qualified Pulsed Electric Thruster for Satellite Control", Journal of Spacecraft and Rockets, Vol 11, No. 9, Sep 1974, pp. 613-617.

APPENDIX C.

CRITICAL SPEED FOR SELF-FIELD PLASMA THRUSTERS

## CRITICAL SPEED FOR SELF-FIELD PLASMA THRUSTERS

### C.1. INTRODUCTION

For several years, it has been suggested that the exhaust velocity of a magnetoplasmadynamic arcjet is limited by the so-called Alfvén critical speed:

$$u_{\text{crit}} = \left( \frac{2E}{m} \right)^{1/2}$$

where  $E$  is the first ionization level of a fuel atom of mass  $m$ . A few theories, based on quite different physical models, have led to this speed as a characteristic value of the exhaust velocity at which electrode erosion, insulator ablation, and/or "plasma instabilities" develop that serve to limit arcjet performance. In particular, for arcjet current  $J$  and mass flow  $\dot{m}$ , the "onset" of difficulties appears to occur at values of  $J^2/\dot{m}$  that result in exhaust speeds near Alfvén critical speed. The present discussion invokes the electromagnetic structure of the discharge flow and a requirement for power balance in steady-state in order to derive self-consistent mass flow rates and exhaust speeds.

### C.2. MODEL

The basic equation for the current distribution in a plasma flow is:

$$\frac{D_e}{D_t} \left( \frac{\bar{B}}{\rho} \right) = \frac{v^2 \bar{B}}{\rho \sigma u}$$

where  $\rho$  = mass density,  $\sigma$  = electrical conductivity (assumed constant), and the convective derivative is based on the electron fluid velocity  $\bar{u}_e$ . (For high density flows, the plasma flow velocity may be substituted for  $\bar{u}_e$ ). By dimensional analysis, the characteristic scale over which the magnetic field varies through the plasma flow in steady state is:

$$\delta = \frac{1}{\sigma \rho u}$$

Without flow, the magnetic field would decrease linearly between

the upstream and downstream boundaries of the thruster. As the conducting flow accelerates, it convects magnetic flux away from the upstream region and concentrates flux near the downstream ( $B=0$ ) boundary. A bifurcated current density distribution is thereby obtained. Higher flow speeds result in greater current concentration, and more intense dissipation. The consequence of such dissipation is increased ablation of electrodes and insulators. Ablation, however, contributes to the total mass flow rate and thereby lowers the flow speed, reducing the current concentration. A self-consistent solution should therefore be expected.

As a simple model, let convection provide the primary mechanism balancing resistive dissipation, with ablation absorbing the heat not carried away by the fuel mass flow:

$$\dot{m}_A Q_A = \epsilon \left[ \frac{j^2 v}{\sigma} - \dot{m}_F Q_F \right]$$

where  $j$  = current density

$v$  = volume in which dissipation occurs

$\dot{m}$  = mass flow rate

$Q$  = heat absorbed per unit mass.

Subscripts A and F refer to ablated and fuel mass, respectively. The factor  $\epsilon$  allows energy to be lost without causing ablation (e.g., radiation to free space, thermal conduction).

The current density may be written in terms of the total current  $J$  and the characteristic scale  $\delta$ , which also provides the volume, so

$$\begin{aligned} \frac{j^2}{\sigma} v &= \frac{1}{\sigma} \left( \frac{J}{2\pi r \delta} \right)^2 \pi r^2 \delta g \\ &= \left( \frac{\mu}{4\pi} \right) J^2 u g \end{aligned}$$

where  $g$  is a geometric factor that depends on the particular thruster, and  $u$  is the exhaust speed. The electromagnetic thrust provides this speed:

$$u = \frac{\mu}{4\pi} \frac{j^2}{\dot{m}} \ln r_2/r_1 + \frac{3}{4}$$

where  $m$  is the total mass flow rate  $\dot{m}_F + \dot{m}_A$ . Substitution in the equation for ablation results in a quadratic equation:

$$(\dot{m}_F + \dot{m}_A) \dot{m}_F Q_F + \dot{m}_A \frac{Q_A}{\epsilon} = \frac{\mu}{4\pi} J^2 g \ln \frac{r_2}{r_1} + \frac{3}{4}$$

The ablation rate relative to the fuel flow rate is then:

$$\alpha = \frac{\dot{m}_A}{\dot{m}_F} = \frac{[(\alpha+1)^2 + 4\alpha(\beta-1)]^{1/2} - (\alpha+1)}{2\alpha}$$

where  $\alpha = Q_A/\epsilon Q_F$

and

$$\beta = \frac{\mu}{4\pi} \frac{J^2}{\dot{m}_F} \frac{2}{Q_F} g(\ln r_2/r_1 + 3/4)$$

For  $\beta < 1$ , there is no physical solution for the model as constructed. There is insufficient dissipation to account for the heat that could be carried away by the injected mass flow rate absorbing an energy per unit mass  $Q_F$ . This insufficiency can be resolved simply by reducing  $Q_F$ , i.e., allowing incomplete ionization of the injected flow. For  $\beta > 1$  the fuel mass flow cannot cool the thruster sufficiently and ablation occurs. The degree of ablation and thus the exhaust velocity attained for a given current flow depends on the heat that can be absorbed by the ablated material, expressed relative to the fuel by the parameter  $\alpha$ .

The condition  $\beta=1$  provides a value for  $J^2/\dot{m}_F$  for which  $\dot{m}_A = 0$  and the dissipation is exactly balanced by convection in the fuel mass flow. This value of  $J^2/\dot{m}_F$  substituted in the equation for exhaust velocity gives:

$$u = u_0 = [Q_F g(\ln r_2/r_1 + 3/4)]^{1/2}$$

for  $Q_F \approx E/m$  and  $g(\ln r_2/r_1 + 3/4) \approx 2$ ,  $u_0 \approx u_{crit}$ . Thus, correlation of self-field plasma thruster performance with

Alfven critical speed might be expected simply on the basis of ablation when the fuel flow rate is insufficient for thruster cooling.

In Fig C-1, the actual exhaust speed (i.e., with ablation) is compared with  $u_I$ , the ideal exhaust speed (no ablation), as the ideal speed is increased relative to  $u_0$ . If there is no possibility of ablation ( $\alpha=0$ ), then the exhaust speed can increase indefinitely. In the presence of plasma at 1-3 eV, however, solid surfaces can be expected to ablate and ionize about as readily as neutral fuel gas ( $\alpha \sim 1$ ). Thus, a little excess heating is rapidly compensated by additional mass flow, resulting in an exhaust speed "plateau" at about  $u_0 \approx u_{crit}$ .

For  $\alpha=0$ , which would correspond to an ablation-fed thruster, Fig C-1 indicates that the exhaust speed decreases relative to  $u_0$  based on  $Q_F$ . Proper substitution of this limiting case ( $\dot{m}_F=0$ ) in the ablation cooling model, however, provides a constant operating speed:

$$u_A = Q_A g \left( \ln \frac{r_2}{r_1} + \frac{3}{4} \right)^{1/2}$$

that is basically equivalent to operation at  $\beta=1$ . The characteristic discharge thickness for an ablation arc is then:

$$r_A = \frac{1}{\rho u_A}$$

### C.3. EXOTHERMIC ABLATION

For exothermic vs endothermic propellant slabs, there would be a modest reduction of  $Q_A$ , which is dominated by the several eV needed to ionize vs the tenths of eV needed to ablate atoms from a surface. The pressure in the gas phase of propellant combustion would typically be too high to maintain sufficient ionization and electron temperature so the electrical conductivity would be too low for current conduction near

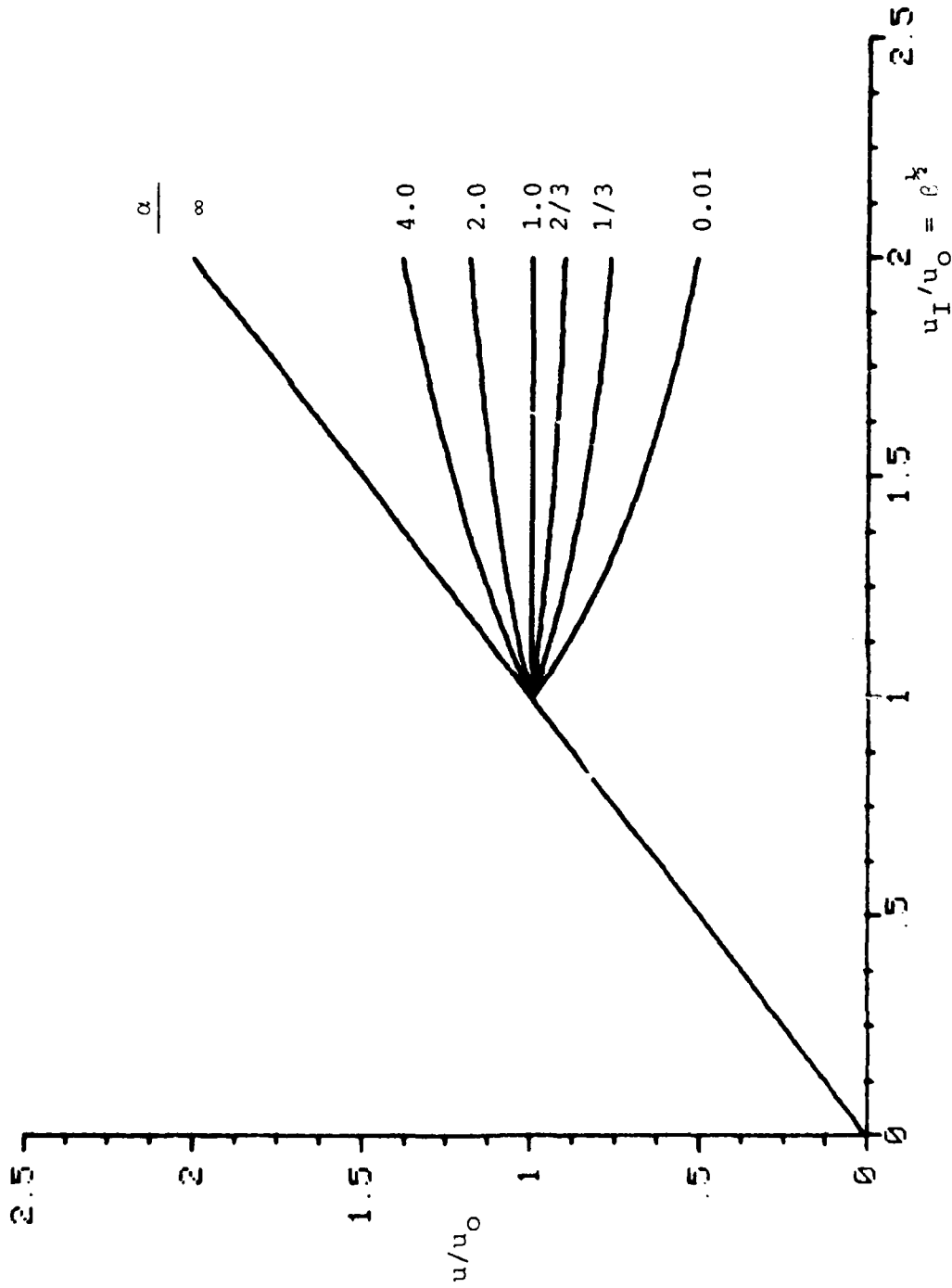


FIGURE C-1. Variation of actual speed with expected speed, both relative to critical speed  $u_0$ , as function of energy per unit mass for ablation relative to fuel,  $\alpha = Q_A/\epsilon Q_F$ .

the surface. If the thruster chamber geometry allowed high chamber pressures, then current flow within the chamber might also be prevented. In the present model, resistive heating is the only source of energy for ablation. With exothermic propellants, however, not only is  $Q_A$  reduced, but ablation can proceed even if the current density near the surface decreases to zero ( $\delta \rightarrow$  large, associated with  $u \rightarrow$  small). The ablation arc could then be blown out of the thrust chamber. Burning of propellant in a less-confined arrangement might allow current flow and ionization in the lower pressure flow downstream of the propellant surface. (In the diffusive limit, the current density distribution will be determined by the conductivity distribution). Adjusting  $Q_A$  and the chamber geometry to allow ablation arc operation would provide lower values of specific impulse and higher thrust per watt of electrical power.

#### C.4. CONCLUDING REMARKS

The present ablation cooling model provides a simple physical basis for understanding velocity limitations in self-field plasma thrusters without invoking a priori conditions such as minimum power operation or choking. If additional physics could provide a relationship between the efficiency of heat transfer to ablation,  $\epsilon$ , and the current scale length  $\delta$ , then it might be possible to explain the voltage oscillations characteristic of "onset". For example, suppose  $\epsilon = 1$  for  $\delta < \delta_{th}$ , a diffusion distance for heat transfer from the plasma and  $\epsilon = 0$  for  $\delta > \delta_{th}$ . At a high enough value of  $u_I/u_0$ , the actual exhaust velocity might alternate between values corresponding to two different values of  $\alpha$ . The corresponding variation in back EMF ( $u \times B$ ) voltage would be observed as voltage oscillations in the thruster terminal characteristics and noise on electrostatic probes. The characteristic time scale for such fluctuations would be associated with the change in flow field through the thruster, i.e., the thruster depth divided by the exhaust speed, ( $d/u \approx 5 \text{ cm}/1.5 \times 10^4 \text{ m/s} = 3.3 \text{ } \mu\text{sec}$ ). Oscillations at several hundred kilohertz should be observed.

END

9-87

DTIC